Quasinormal modes and bound states of massive scalar fields in wormhole spacetimes

Sebastián Alfaro[1,*] P. A. González,[2,†] Diego Olmos[1,‡]
Eleftherios Papantonopoulos,[3,§] and Yerko Vásquez[1,∥]

[1]*Departamento de Física, Facultad de Ciencias, Universidad de La Serena,*
Avenida Cisternas 1200, La Serena, Chile
[2]*Facultad de Ingeniería y Ciencias, Universidad Diego Portales,*
Avenida Ejército Libertador 441, Casilla 298-V, Santiago, Chile
[3]*Physics Division, School of Applied Mathematical and Physical Sciences,*
National Technical University of Athens, 15780 Zografou Campus, Athens, Greece

In this work we explore the propagation of massive scalar fields on some wormhole backgrounds. On one side, we consider the Bronnikov-Ellis wormhole solution and wormhole geometries with a nonconstant redshift function by introducing a gravitational mass M, which goes over into the Bronnikov-Ellis wormhole when the gravitational mass parameter vanishes. We employ the continued fraction method to calculate accurately the quasinormal frequencies of massive scalar fields, particularly focusing on low values of the angular number, and we show an anomalous behavior of the decay rate of the quasinormal frequencies, for $n \geq \ell$. Also, we show that for a massive scalar field and $M \neq 0$ the effective potential allows potential wells for some values of the parameters which support bound states, which are obtained using the continued fraction method and they are characterized by having only a frequency of oscillation and they do not decay; however, for the Bronnikov-Ellis wormhole the effective potential do not support bound states. On the other side, we consider a wormhole geometry which is an exact solution of $f(R)$ modified gravity. For this geometry the quasinormal frequencies can be obtained analytically, being the longest-lived modes the ones with lowest angular number ℓ. So, in this wormhole background the anomalous behavior is avoided.

I. INTRODUCTION

Solutions of Einstein equations that connect different parts of the Universe or two different Universes can be found in general relativity (GR) known as wormholes. The concept of the wormhole can be traced back to Flamm in 1916 [1] and then wormhole-type solutions were found by Einstein and Rosen, where they considered a physical space representing a physical space which was connected by a wormhole-type solution known as the Einstein-Rosen bridge [2]. Then, the pioneering work of Misner and Wheeler [3] and Wheeler [4] developed further the wormholes concept. Lorentzian wormholes were studied in GR [5–9], in which conditions for traversable wormholes were found introducing a static spherically symmetric metric. However, a condition on the wormhole throat leads

to the violation of the null energy condition (NEC). To allow the formation of traversable wormhole geometries a matter distribution of exotic or phantom matter has to be introduced [8].

Recently there are many efforts to understand modifications of GR which are generated by the presence of a scalar field coupled to gravity. This coupling has important implications in local and global solutions in these theories known as scalar-tensor theories [10]. One of the best studied scalar-tensor theories is provided by the Horndeski Lagrangian [11]. The Horndeski theory has been studied in short and large distances. In this theory black hole solutions were found [12–16], known as Galilean black holes, and also wormhole geometries were generated [17–23].

A study of Galileon black holes was performed in [24]. The Regge-Wheeler potential generated by a test wave in the vicinity of a Galileon black hole potential was studied and it was investigated the formation and the behavior of bound states trapped in this potential well or penetrating the horizon of the Galileon black hole. The formation of the bound states was depending of how strongly matter is coupled to gravity expressed by the coupling the scalar

*sebastian.alfaroz@userena.cl
†pablo.gonzalez@udp.cl
‡diego.olmos@userena.cl
§lpapa@central.ntua.gr
∥yvasquez@userena.cl

104009-1

field to Einstein tensor. In [25] bound states in a wormhole geometry in the scalar-tensor Horndeski theory were studied in which the wormhole throat connects two anti–de Sitter (AdS) spacetimes. The scalar field is coupled kinetically to curvature and exact static spherically symmetric wormhole solutions were found. Using the Wentzel-Kramers-Brillouin (WKB) approximation the formation and propagation of bound states in the vicinity of a wormhole was studied. The behavior of the bound states trapped in the potential wells and the flow between the two AdS regions was investigated.

An important issue of the compact objects formed by black holes or wormholes is their stability. The relativistic collision of two of these compact objects produces gravitational waves which will help us to understand better the gravitational interaction. However, the recent LIGO detections [26–30] do not yet probe the detailed structure of spacetime beyond the photon sphere. Future observations may detect the ringdown phase, which is governed by a series of damped oscillatory modes at early times, which are known as quasinormal modes (QNMs) [31–38]. Future gravitational observations may provide information on different compact objects than black holes, objects without event horizons which are known as exotic compact objects [34–39]. Perturbations of black holes and wormholes were extensively studied in the literature. In the case that a test scalar perturbs black hole compact objects the partially reflected waves from the photon sphere mirror off the AdS boundary and reperturb the photon sphere to give rise to a damped beating pattern. In the case of a wormhole do not decay with time but have constant and equal amplitude to that of the initial ringdown. Therefore, the knowledge of QNMs and quasinormal frequencies (QNFs) can give us important information on the properties of compact objects and distinguish their nature. The QNMs give an infinite discrete spectrum which consists of complex frequencies, $\omega = \omega_R + i\omega_I$, where the real part ω_R determines the oscillation timescale of the modes, while the complex part ω_I determines their exponential decaying timescale (for a review on QNMs see [32,33]).

In the case that the probe scalar field is massive, a new mass scale is introduced and then a different behavior was found [40–43], at least for the overtone $n = 0$. If the mass of the scalar field is light, then the longest-lived QNMs are those with a high angular number ℓ, whereas if the mass of the scalar field is large the longest-lived modes are those with a low angular number ℓ. One is expecting this behavior because the fluctuations of the probe massive scalar field can maintain the QNMs to live longer even if the angular number ℓ is large, introducing in this way an anomaly of the decaying modes depending on the mass of the scalar field exceeding a critical value or not. Also, if a cosmological constant is introduced an anomalous behavior of QNMs was found in [44] because there is interplay of the mass of the scalar field and the value of the cosmological

constant. If the background metric is the Reissner-Nordström and the probe scalar field is massless [45] of massive [46] depending on critical values of the charge of the black hole, the charge of the scalar field and its mass an anomalous behavior was also found. The decay modes of QNMs in various setups were studied in [47–52].

QNMs and QNFs have also been calculated in the background of wormholes. The perturbations of wormhole spacetime was investigated in [53]. It was found that the QNMs behave the same way as in black hole background and includes the quasinormal ringing and power-law asymptotically late time tails. However, in [54] it was found that the symmetric wormholes do not have the same ringing behavior of the black holes at a few various dominant multipoles. In the case of massive probe scalar field perturbations, it was shown [55] that wormholes with a constant redshift function do not allow for longest-lived modes, while wormholes with nonvanishing radial tidal force do allow for quasiresonances. Calculating the high frequency QNMs in the case of the Morris-Thorne wormhole spacetime, the shape function of a spherically symmetric traversable Lorenzian wormhole near its throat was constructed in [56]. Scalar and axial QNMs of massive static phantom wormholes were calculated in [57].

In [58] it was shown that if the probe scalar field is massive then an anomalous behavior of QNMs was also observed if the background metric defines a wormhole geometry. It was shown that in the case of Bronnikov-Ellis wormhole [6] there is a critical mass of the scalar field beyond which the anomalous decay rate of the QNMs is present. In the case of the Morris-Thorne wormhole [35] the anomalous decay rate of the QNMs is not present at least for the fundamental modes. In [59] polar perturbations of static Bronnikov-Ellis wormholes were studied and the QNMs of rapidly rotating Bronnikov-Ellis wormholes were recently analyzed in [60].

As we already discussed in the case of the Horndeski scalar-tensor theory if matter, parametrized by a phantom scalar field, is strongly coupled to gravity then bound states are formed [24,25]. In this work we follow a much simpler approach. We consider the Bronnikov-Ellis wormhole solution [5,6] and wormhole geometries with nonconstant redshift function by introducing a gravitational mass M, which goes over into the Bronnikov-Ellis wormhole when $M = 0$. We perturb the massive wormhole background by a test massive scalar field. Using the continued fraction method we calculate accurately the QNFs for low values of the angular number. We find stability of the background wormhole and calculating the effective potential we show that for an interplay of the mass parameter and the phantom scalar charge, potential wells are generated supporting bound states.

We also study the QNFs in a wormhole spacetime supported by a phantom scalar field in which the scalar curvature is generalized to an $f(R)$ function [61–65]. In this

model the scalar field self-interacts with a mass term potential which is derived from the scalar equation and in the resulting $f(R)$ model the scalar curvature is modified by the presence of the scalar field and it is free of ghosts and avoids the tachyonic instability.

The work is organized as follows. In Sec. II we review the solutions of the traversable wormholes. In Sec. III we study the perturbations of massive scalar field in the wormhole geometry. In Sec. IV we calculate the QNFs of the nonconstant redshift function wormholes, resulting in a nonzero tidal radial force, and the Bronnikov-Ellis wormhole numerically using the continued fraction method. Also, we show that bound states are allowed by the wormholes with nonvanishing radial tidal force and the frequencies of the lowest bound states are calculated using the continued fraction method. In Sec. V we calculate the QNFs of an $f(R)$ gravity wormhole analytically and using the WKB method. In Sec. VI are our conclusions.

II. REVIEW OF TRAVERSABLE WORMHOLES

Morris and Thorne [7] were the first they found the necessary conditions, for a static spherically symmetric metric, to generate traversable Lorentzian wormholes as exact solutions in GR. To find a solution, conditions on the wormhole throat necessitate the introduction of exotic matter, which leads to the violation of the NEC.

We consider the following action

$$S = \int d^4x \sqrt{-g} \left(\frac{R}{2} + \frac{1}{2} \partial^\mu \phi \partial_\mu \phi - V(\phi) \right), \quad (1)$$

which consists of the Ricci scalar R, a scalar field with negative kinetic energy and a self-interacting potential. The field equations that emerge through the variation of this action are

$$R_{\mu\nu} - \frac{1}{2} g_{\mu\nu} R = T^\phi_{\mu\nu}, \quad (2)$$

$$\Box \phi + V_\phi(\phi) = 0, \quad (3)$$

where $\Box = \nabla^\mu \nabla_\mu$ represents the D'Alambert operator with respect to the metric, and the energy-momentum tensor is given by

$$T^\phi_{\mu\nu} = -\partial_\mu \phi \partial_\nu \phi + \frac{1}{2} g_{\mu\nu} \partial^\alpha \phi \partial_\alpha \phi - g_{\mu\nu} V(\phi). \quad (4)$$

We consider the metric ansatz proposed by Morris and Thorne [7] in spherical coordinates, which is given by

$$ds^2 = -e^{2\Phi(r)} dt^2 + \left(1 - \frac{b(r)}{r} \right)^{-1} dr^2 + r^2 d\Omega, \quad (5)$$

where $\Phi(r)$ is the redshift function, $b(r)$ is the shape function and $d\Omega = d\theta^2 + \sin(\theta)^2 d\varphi^2$. To achieve a

wormhole geometry, it is necessary for these functions to adhere to the following conditions [7,9]

(1) $\frac{b(r)}{r} \leq 1$ must hold for every $[r_{\text{th}}, +\infty)$, where r_{th} denotes the radius of the throat. This condition ensures the finiteness of the proper radial distance, defined by $l(r) = \pm \int_{r_{\text{th}}}^r \left(1 - \frac{b(r)}{r} \right)^{-1} dr$, across the entire spacetime. Note that in the coordinates (t, l, θ, φ) the line element (5) can be expressed as

$$ds^2 = -e^{2\Phi(l)} dt^2 + dl^2 + r^2(l)(d\theta^2 + \sin^2 \theta d\varphi^2). \quad (6)$$

Here, the throat radius corresponds to $r_{\text{th}} = \min\{r(l)\}$.

(2) $\frac{b(r_{\text{th}})}{r_{\text{th}}} = 1$ at the throat. This condition arises from the requirement that the throat constitutes a stationary point of $r(l)$. Alternatively, it can be derived from the demand that the embedded surface of the wormhole be vertical at the throat.

(3) $b'(r) < \frac{b(r)}{r}$ which reduces to $b'(r_{\text{th}}) \leq 1$ at the throat. This condition, known as the flare-out condition, guarantees that r_{th} is indeed a minimum and not any other type of stationary point.

To ensure the absence of horizons and singularities requires $\Phi(r) \neq 0$ which means that $\Phi(r)$ is finite throughout the spacetime. The Ellis [6] is a wormhole solution of an action that consists of a pure Einstein-Hilbert term and a scalar field with negative kinetic energy

$$S = \int d^4x \sqrt{-g} \left(\frac{R}{2} + \frac{1}{2} \partial^\mu \phi \partial_\mu \phi \right). \quad (7)$$

Given the metric ansatz (5) and setting $V(r) = 0$, the aforementioned equations yield the following solution

$$\Phi(r) = 0, \quad (8)$$

$$b(r) = A^2/r, \quad (9)$$

$$\phi(r) = \sqrt{2} \tan^{-1} \left(\frac{\sqrt{r^2 - A^2}}{A} \right) + \phi_\infty, \quad (10)$$

$$R(r) = -\frac{2A^2}{r^4}, \quad (11)$$

where A, ϕ_∞ are constants of integration. The spacetime is asymptotically flat, which is evident in the behavior of $b(r)$ and $R(r)$. The wormhole throat is determined by the solution of the equation

$$g_{rr}^{-1} = 0 \rightarrow r_{\text{th}} = \pm A. \quad (12)$$

Additionally, the solution satisfies the flare-out condition, and it meets the requirement $b'(r_{\text{th}}) = -1$.

A constant value at infinity $\phi(r \to \infty) = \frac{\pi}{\sqrt{2}} + \phi_\infty$ has scalar field takes, so to make the scalar field vanish at large distances we will set $\phi_\infty = -\frac{\pi}{\sqrt{2}}$. The scalar field takes the asymptotic value at infinity at the position of the throat $\phi(r = r_{\text{th}}) = \phi_\infty$. From the solution one can see in (9), (10) and (11) the integration constant A of the phantom scalar field plays a very important role in the formation of the wormhole geometry. It has units $[L]^2$, appears in the scalar curvature and at the position of the throat takes the value $R_{r=r_{\text{th}}}(A) = -2/A^2$. Also it effects the size of the throat, a larger charge A gives a larger wormhole throat. The above discussion indicates that the phantom scalar field is very important for the generation of the wormhole geometry and to define the scalar curvature and specifying the throat of the wormhole geometry.

The function $b(r)$ encodes the shape of the wormhole and at certain minimum value of r, the throat of a wormhole is defined, namely, when $r_{\text{min}} = b_0$. Thus, the radial coordinate increases ranging from r_{min} until spatial infinity $r = \infty$. Also $\Phi(r)$ must be finite everywhere in light of the requirement of absence of singularities. In addition, $\Phi(r) \to 0$ as $r \to \infty$ (or $l \to \pm\infty$) based on the requirement of asymptotic flatness. On the other hand, the shape

function $b(r)$ should satisfy that $1 - b(r)/r > 0$ and $b(r)/r \to 0$ as $r \to \infty$ (or equivalently $l \to \pm\infty$). In the throat $r = b(r)$ and thus $1 - b(r)/r$ vanishes. Traversable wormholes do not have a singularity in the throat. The latter means that travelers can pass through the wormhole during the finite time.

We will consider the following metric functions

$$e^{2\Phi(r)} = 1 - \frac{2M}{r}, \qquad b(r) = \frac{b_0^2}{r}, \qquad (13)$$

which corresponds to the Bronnikov-Ellis wormhole in the limit $M \to 0$ [5,6]. Note that the parameter b_0 specifies the charge of the phantom scalar field.

The most general energy-momentum tensor compatible with wormhole geometries is given by [66]

$$T_\nu^\mu = \text{diag}(-\rho, p_r, p_t, p_t), \qquad (14)$$

where ρ denotes the energy density, and p_r and p_t represent the radial and tangential pressures, respectively.

The Einstein field equations take the form

$$\rho = \frac{b'(r)}{r^2},$$

$$p_r = \frac{-b(r) + 2r(r - b(r))\Phi'(r)}{r^3},$$

$$p_t = \frac{(b(r) - rb'(r) + 2r(r - b(r))\Phi'(r))(1 + r\Phi'(r)) + 2(r - b(r))r^2\Phi''(r)}{2r^3}.$$

The important energy conditions include the weak energy condition (WEC), the NEC, the strong energy condition (SEC) and the dominant energy condition (DEC). These conditions, expressed in terms of the principal pressures, are given by the following see for instance [67]:

$$\text{WEC:} \ \rho \geq 0, \rho + p_r \geq 0, \rho + p_t \geq 0,$$

$$\text{NEC:} \ \rho + p_r \geq 0, \rho + p_t \geq 0,$$

$$\text{SEC:} \ \rho + p_r \geq 0, \rho + p_t \geq 0, \rho + p_r + 2p_t \geq 0,$$

$$\text{DEC:} \ \rho \geq 0, \rho - |p_r| \geq 0, \rho - |p_t| \geq 0.$$

For the wormhole geometry (13), the obtained expressions are as follows:

$$\rho = -\frac{b_0^2}{r^4}, \qquad p_r = \frac{-b_0^2 + 2Mr}{r^3(r - 2M)}, \qquad p_t = \frac{(b_0^2(M - r) + Mr^2)}{r^4(r - 2M)^2},$$

$$\rho + p_r = \frac{2(b_0^2(M - r) + Mr^2)}{r^4(r - 2M)}, \qquad \rho + p_t = \frac{M(b_0^2(2r - 3M) + (M - r)r^2)}{r^4(r - 2M)^2}.$$

Hence, $\rho < 0$, leading to the violation of the WEC for any $r > r_{\text{th}} = b_0$. Furthermore, in the range $b_0 \leq r < \frac{b_0^2 + \sqrt{b_0^4 - 4b_0^2 M^2}}{2M}$, $\rho + p_r$ is negative. Additionally, p_t becomes negative for $r > \frac{b_0^2 + \sqrt{b_0^4 - 4b_0^2 M^2}}{2M}$. Consequently, this implies that $\rho + p_t$ is at least negative in that range. Consequently, all the energy conditions are violated for $r > r_{\text{th}}$.

III. MASSIVE SCALAR FIELD PERTURBATIONS

To investigate the propagation of a massive scalar field in a wormhole geometry, we consider the Klein-Gordon equation, which is expressed as

$$\frac{1}{\sqrt{-g}}\partial_\mu(\sqrt{-g}g^{\mu\nu}\partial_\nu)\Psi = m^2\Psi. \tag{15}$$

To decouple and subsequently solve the Klein-Gordon equation, we employ the method of separation of variables, utilizing the following ansatz

$$\Psi(t,r,\theta,\varphi) = e^{-i\omega t}\frac{u(r)}{r}Y_\ell(\Omega). \tag{16}$$

Here, ω represents the unknown frequency (to be determined), and $Y_\ell(\Omega)$ denotes the spherical harmonics, dependent solely on the angular coordinates [68].

After implementing the aforementioned mentioned ansatz, it becomes straightforward to derive a Schrödinger-like equation for the radial part, specifically

$$\frac{d^2u}{dr^{*2}} + [\omega^2 - V(r^*)]u = 0, \tag{17}$$

where r^* is the well-known tortoise coordinate, i.e.,

$$r^* \equiv \int \frac{dr}{e^\Phi\sqrt{1-\frac{b(r)}{r}}}. \tag{18}$$

Finally, the effective potential for scalar field perturbations is given by

$$V(r) = e^{2\Phi}\left(m^2 + \frac{\ell(\ell+1)}{r^2} - \frac{b'r-b}{2r^3} + \frac{1}{r}\left(1-\frac{b}{r}\right)\Phi'\right), \tag{19}$$

FIG. 1. Effective potential of the wormhole spacetime (13), for $M/b_0 = 0.25$, $mb_0 = 0.8$ and $\ell = 0, 1, 2$.

where the prime denotes differentiation with respect to the radial coordinate and $\ell \geq 0$ is the angular degree. Therefore, we have transformed the problem into the well-known one-dimensional Schrödinger equation with energy ω^2 and an effective potential $V(r)$.

IV. BRONNIKOV-ELLIS WORMHOLES AND NONCONSTANT REDSHIFT FUNCTION WORMHOLES

We consider the following metric functions

$$e^{2\Phi(r)} = 1 - \frac{2M}{r}, \qquad b(r) = \frac{b_0^2}{r}, \tag{20}$$

which goes over into the Bronnikov-Ellis wormhole in the limit $M \to 0$. Thus, the effective potential of scalar perturbations is given by

$$V(r) = \frac{-3Mq^2 + q^2r + (1 - 2\ell(\ell+1))Mr^2 + \ell(\ell+1)r^3}{r^5} + \left(1 - \frac{2M}{r}\right)m^2, \tag{21}$$

which is plotted in Fig. 1, where a barrierlike shape is observed. Additionally, a well may form near the throat for a massive scalar field, $M \neq 0$ and at low values of ℓ, while for high values of ℓ, the well disappears; therefore, the potential can support bound states for low values of ℓ.

For $M = 0$ the effective potential transforms into $V(r) = q^2/r^4 + \ell(\ell+1)/r^2 + m^2$, and it is straightforward to demonstrate that it cannot give rise to a well; hence, bound states are prohibited in this case.

On the other hand, Eq. (17) can be written as

$$(2M - r)(b_0^2 - r^2)u''(r) + \frac{(-3Mb_0^2 + Mr^2 + b_0^2r)}{r}u'(r)$$

$$+ \frac{M((2m^2r^2 + 2\ell^2 + 2\ell - 1)r^2 + 3b_0^2) - r(r^2(\ell^2 + \ell + r^2(m^2 - \omega^2)) + b_0^2)}{r^2}u(r) = 0, \tag{22}$$

which we will solve numerically to determine both the QNFs and the frequencies of bound states.

A. Quasinormal frequencies

In this section we use the continued fraction method (CFM) to calculate accurately the QNFs for massive scalar fields propagating on the Bronnikov-Ellis wormhole and nonconstant redshift function wormholes described by Eq. (13). The CFM was devised by Leaver to compute the QNMs of Schwarzschild and Kerr black holes [69,70], and improved later by Nollert [71]. It has been used to computed the QNMs in several black holes backgrounds, see for instance [72–76]. However, to our knowledge this is the first time that this method is applied to calculate the QNFs in wormhole geometries.

To solve the radial equation it is necessary to specify the boundary conditions. Given the asymptotically flat nature of the wormhole geometries and the fact that the effective potential forms a barrier approaching $V(r^*) \to m^2$ as $r^* \to \pm\infty$, we will consider the boundary conditions that demand purely outgoing waves at both infinities. In other words, no waves are coming from either asymptotically flat region [53,77]

$$\Psi \sim e^{i\sqrt{\omega^2-m^2}r^*}, \qquad r^* \to +\infty.$$

$$\Psi \sim e^{-i\sqrt{\omega^2-m^2}r^*}, \qquad r^* \to -\infty. \tag{23}$$

However, for the CFM it is more convenient to implement boundary conditions at the throat and at infinity taking into account the symmetry of the potential, as it is explained next. Therefore, the boundary condition that there are only outgoing waves at infinity is satisfied by the radial solution

$$u \sim e^{i\Omega r^*} \quad \text{as } r^* \to \infty,$$

where $\Omega = \sqrt{\omega^2 - m^2}$, which can be rewritten as

$$u \sim e^{i\Omega r}r^{iM\omega^2/\Omega} \quad \text{as } r \to \infty. \tag{24}$$

Also, since the potential is symmetric about the throat of the wormhole, which is located at $r_0^* = 0$, the solutions will be symmetric or antisymmetric. Therefore, we impose the following boundary conditions at the throat, $\frac{du}{dr^*}\big|_{r_0^*} = 0$ for the symmetric solutions and $u(r_0^*) = 0$ for the antisymmetric solutions. These boundary conditions yields the even and odd overtones, respectively. It is worth mentioning that similar boundary conditions have been applied for other wormhole geometries, where the QNMs were obtained by direct integration of the wave equation [78,79].

It is convenient to consider the following ansatz for the symmetric solutions of the radial equation (22) which satisfies the desired boundary conditions

$$u(r) = e^{i\Omega r}r^{iM\omega^2/\Omega} \sum_{n=0}^{\infty} a_n \left(\frac{r-b_0}{r}\right)^n. \tag{25}$$

So, substituting this expression in the radial equation, the following five-term recurrence relation is satisfied by the expansion coefficients

$$c_0(0)a_1 + c_1(0)a_0 = 0,$$
$$c_0(1)a_2 + c_1(1)a_1 + c_2(1)a_0 = 0,$$
$$c_0(2)a_3 + c_1(2)a_2 + c_2(2)a_1 + c_3(2)a_0 = 0,$$
$$c_0(n)a_{n+1} + c_1(n)a_n + c_2(n)a_{n-1} + c_3(n)a_{n-2} + c_4(n)a_{n-3} = 0, \quad n \geq 3, \tag{26}$$

where

$$c_0(n) = -(n+1)(2n+1)(b_0-2M)(m^2-\omega^2),$$

$$c_1(n) = b_0^3(m^2-\omega^2)^2 - ib_0^2(m^2-\omega^2)\left((4n+1)\sqrt{\omega^2-m^2} - 2im^2M\right) + b_0\left(m^2\left(\ell^2+\ell+n\left(8iM\sqrt{\omega^2-m^2}+5n+2\right)\right.\right.$$
$$\left.+2iM\sqrt{\omega^2-m^2}+1\right) - \omega^2\left(\ell^2+\ell+n\left(4iM\sqrt{\omega^2-m^2}+5n+2\right)+iM\sqrt{\omega^2-m^2}+1\right)\right)$$
$$+2M\left(-(\ell^2+\ell+n(7n+2)+1)(m^2-\omega^2)-4iMn\omega^2\sqrt{\omega^2-m^2}-iM\omega^2\sqrt{\omega^2-m^2}\right),$$

$$c_2(n) = b_0\left(\omega^2\left(n\left(6iM\sqrt{\omega^2-m^2}+4n-3\right)-4iM\sqrt{\omega^2-m^2}+6M^2\omega^2+1\right) - m^2\left(n\left(12iM\sqrt{\omega^2-m^2}+4n-3\right)\right.\right.$$
$$\left.-6iM\sqrt{\omega^2-m^2}+8M^2\omega^2+1\right)\right) + b_0^2(m^2-\omega^2)\left(2m^2M+i(2n-1)\sqrt{\omega^2-m^2}\right) + M\left((2\ell(\ell+1)+n(18n)\right.$$
$$-17)+7)(m^2-\omega^2)+20iMn\omega^2\sqrt{\omega^2-m^2}-8iM\omega^2\sqrt{\omega^2-m^2}+4M^2\omega^4\Big),$$

$$c_3(n) = b_0\left(m^2\left(n\left(4iM\sqrt{\omega^2-m^2}+n-2\right)-5iM\sqrt{\omega^2-m^2}+4M^2\omega^2+1\right)-\omega^2\left(n\left(2iM\sqrt{\omega^2-m^2}+n-2\right)\right.\right.$$

$$- 3iM\sqrt{\omega^2 - m^2} + 3M^2\omega^2 + 1\big)\big) + M\big(-16iMn\omega^2\sqrt{\omega^2 - m^2} + 17iM\omega^2\sqrt{\omega^2 - m^2} - (2n(5n - 11) + 13)$$

$$(m^2 - \omega^2) - 6M^2\omega^4\big),$$

$$c_4(n) = M\big(m^2(n - 2)(2n - 3) + \omega^2\big(n\big(4iM\sqrt{\omega^2 - m^2} - 2n + 7\big) - 7iM\sqrt{\omega^2 - m^2} + 2M^2\omega^2 - 6\big)\big). \tag{27}$$

On the other hand, for the antisymmetric solutions it is convenient to define

$$u(r) = (r - b_0)^{1/2} e^{i\Omega r} r^{iM\omega^2/\Omega - 1/2} \sum_{n=0}^{\infty} a_n \left(\frac{r - b_0}{r}\right)^n, \tag{28}$$

which incorporates the desired boundary conditions. Thus, substituting this expression in the radial equation, also a five-term recurrence relation (26) is satisfied by the expansion coefficients, but now the coefficients are given by

$$c_0(n) = -4(n + 1)(2n + 3)(b_0 - 2M)(m^2 - \omega^2),$$

$$c_1(n) = b_0\big(m^2\big(4\ell(\ell + 1) + 4n\big(8iM\sqrt{\omega^2 - m^2} + 5n + 7\big) + 24iM\sqrt{\omega^2 - m^2} + 13\big) - \omega^2\big(4\ell(\ell + 1)$$

$$+ 4n\big(4iM\sqrt{\omega^2 - m^2} + 5n + 7\big) + 12iM\sqrt{\omega^2 - m^2} + 13\big)\big) - 4b_0^2(m^2 - \omega^2)\big(2m^2M + i(4n + 3)\sqrt{\omega^2 - m^2}\big)$$

$$+ 4b_0^3(m^2 - \omega^2)^2 + 2M\big(-(4\ell(\ell + 1) + 4n(7n + 9) + 15)(m^2 - \omega^2) - 16iMn\omega^2\sqrt{\omega^2 - m^2} - 12iM\omega^2\sqrt{\omega^2 - m^2}\big),$$

$$c_2(n) = -2b_0m^2\big(2n\big(12iM\sqrt{\omega^2 - m^2} + 4n + 1\big) + 16M^2\omega^2 + 1\big) + 2b_0\omega^2\big(2n\big(6iM\sqrt{\omega^2 - m^2} + 4n + 1\big)$$

$$- 2iM\sqrt{\omega^2 - m^2} + 12M^2\omega^2 + 1\big) + 8b_0^2(m^2 - \omega^2)\big(m^2M + in\sqrt{\omega^2 - m^2}\big) + 4M\big((2\ell(\ell + 1) + 18n^2 + n + 3)$$

$$(m^2 - \omega^2) + 20iMn\omega^2\sqrt{\omega^2 - m^2} + 2iM\omega^2\sqrt{\omega^2 - m^2} + 4M^2\omega^4\big),$$

$$c_3(n) = b_0\big(m^2\big(4n\big(4iM\sqrt{\omega^2 - m^2} + n - 1\big) + 4M\big(4M\omega^2 - 3i\sqrt{\omega^2 - m^2}\big) + 1\big) - \omega^2\big(4n\big(2iM\sqrt{\omega^2 - m^2} + n - 1\big)$$

$$- 8iM\sqrt{\omega^2 - m^2} + 12M^2\omega^2 + 1\big)\big) + 2M\big(-32iMn\omega^2\sqrt{\omega^2 - m^2} + 18iM\omega^2\sqrt{\omega^2 - m^2} - (4n(5n - 6) + 9)$$

$$(m^2 - \omega^2) - 12M^2\omega^4\big),$$

$$c_4(n) = 4M\big(m^2(n - 1)(2n - 3) + \omega^2\big(n\big(4iM\sqrt{\omega^2 - m^2} - 2n + 5\big) - 5iM\sqrt{\omega^2 - m^2} + 2M^2\omega^2 - 3\big)\big).$$

For $M = 0$, the coefficients $c_4(n)$ become zero for both symmetric and antisymmetric solutions; hence, the expansion coefficients satisfy four-term recurrence relations for the Bronnikov-Ellis wormhole. Then, after applying Gaussian elimination twice for $M \neq 0$, and once for $M = 0$, the original recurrence relations (26) can be simplified to a three-term relation, taking on the following concise form

$$\alpha_0 a_1 + \beta_0 a_0 = 0,$$

$$\alpha_n a_{n+1} + \beta_n a_n + \gamma_n a_{n-1} = 0, \quad n = 1, 2, \ldots$$

We skip providing the explicit expressions for α_n, β_n and γ_n of the final three-term recurrence relations. Now, according to Leaver [69,70], the recursion coefficients must satisfy the following continued fraction relation for the convergence of the series

$$\beta_0 - \frac{\alpha_0\gamma_1}{\beta_1 -} \frac{\alpha_1\gamma_2}{\beta_2 -} \cdots \frac{\alpha_n\gamma_{n+1}}{\beta_{n+1} -} \cdots = 0. \tag{29}$$

The continued fraction must be truncated at some large index N and the QNFs are obtained solving this equation numerically. In the following figures we show the behavior of $\text{Re}(\omega)b_0$ and $-\text{Im}(\omega)b_0$ for massive scalar field as a function of mb_0 using the CFM, for the fundamental mode, see Figs. 2, 4 and 6, and the first overtone, see Figs. 3, 5 and 7.

For the fundamental QNFs ($n = 0$), we can observe an inverted behavior of $\text{Im}(\omega)b_0$, that is, when $mb_0 > m_c b_0$, $\text{Im}(\omega)b_0$ increases with ℓ, representing an anomalous decay rate of the QNMs. Conversely, for $mb_0 < m_c b_0$, $\text{Im}(\omega)b_0$ decreases with increasing ℓ for $n \geq \ell$. The critical value $m_c b_0$ rises with an increase in the parameter M/b_0, and the frequency of the oscillation increases with both the
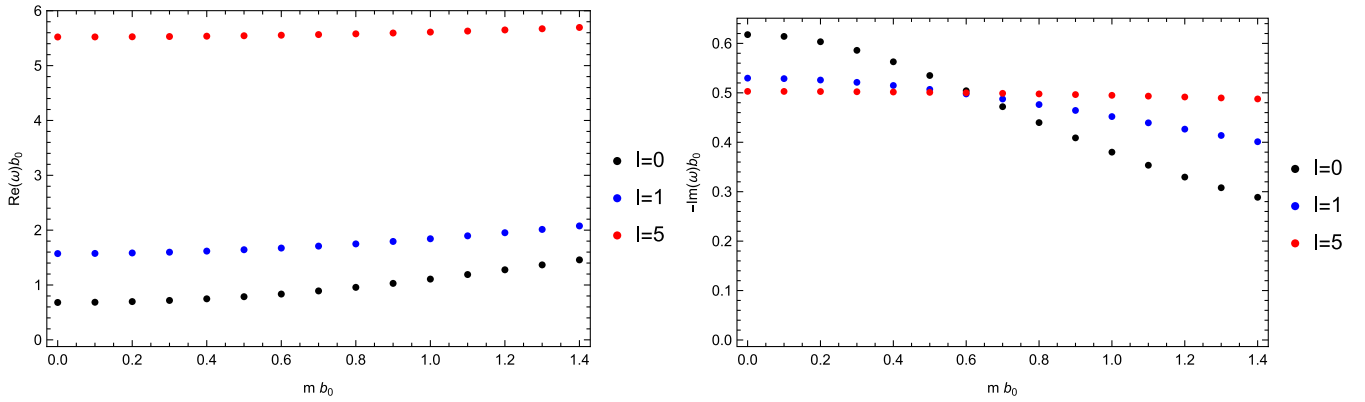
FIG. 2. The behavior of $\mathrm{Re}(\omega)b_0$ and $-\mathrm{Im}(\omega)b_0$ for massive scalar field as a function of mb_0 for the Bronnikov-Ellis wormhole with $n = 0$ (fundamental frequency) and $\ell = 0$, 1, 5 using the CFM.
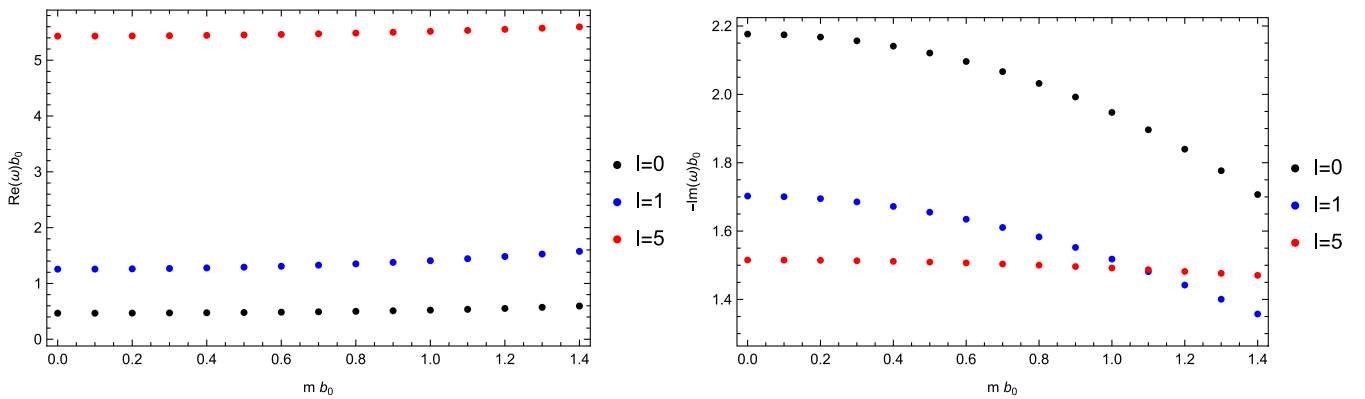
FIG. 3. The behavior of $\mathrm{Re}(\omega)b_0$ and $-\mathrm{Im}(\omega)b_0$ for massive scalar field as a function of mb_0 for the Bronnikov-Ellis wormhole with $n = 1$ (first overtone) and $\ell = 0$, 1, 5 using the CFM.
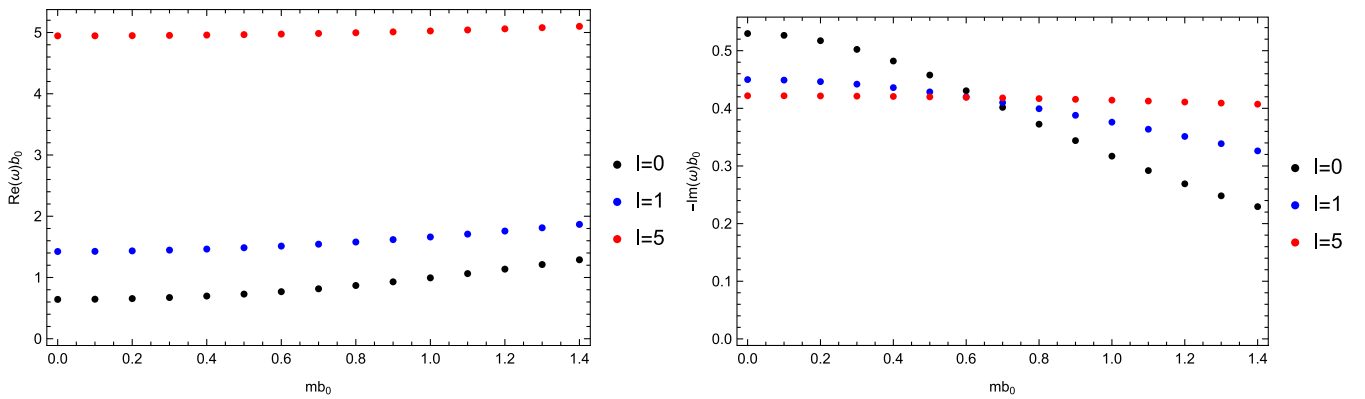
FIG. 4. The behavior of $\mathrm{Re}(\omega)b_0$ and $-\mathrm{Im}(\omega)b_0$ for a massive scalar field as a function of mb_0 for the wormhole spacetime described by Eq. (13), with $M/b_0 = 0.1$, $n = 0$ (fundamental frequency) and $\ell = 0$, 1, 5 using the CFM.

angular number and the parameter mb_0. The frequencies all have a negative imaginary part, which means that the propagation of massive scalar fields is stable in this background. Some numerical values of the QNFs obtained with CFM are in Appendix A. Moreover, in Appendix B we compare the fundamental QNFs and the first overtone using the CFM and the WKB approximation, and we see a good agreement for high values of ℓ as expected, because it is known that the WKB method only yields accurate results for high values of ℓ and for $\ell > n$.
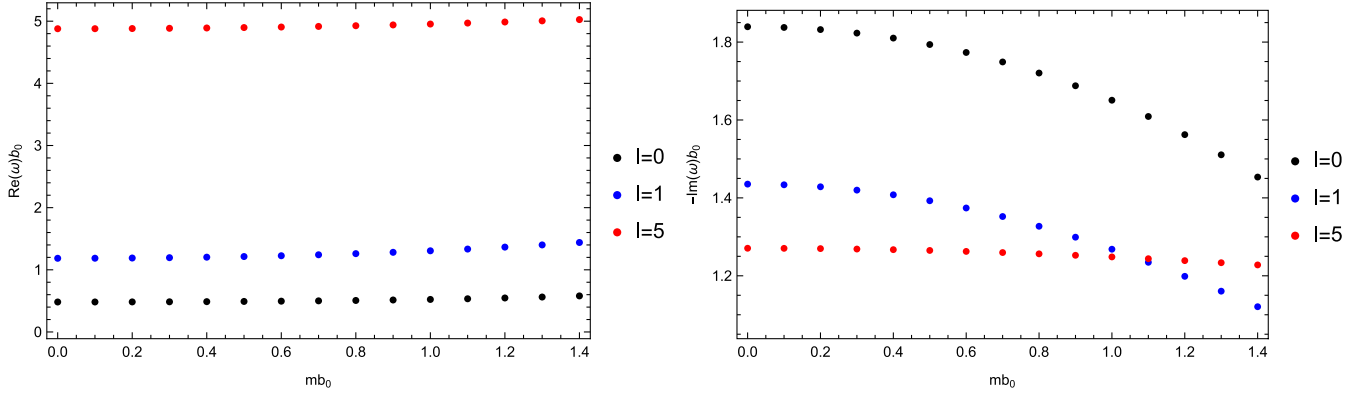
FIG. 5. The behavior of $\mathrm{Re}(\omega)b_0$ and $-\mathrm{Im}(\omega)b_0$ for a massive scalar field as a function of mb_0 for the wormhole spacetime described by Eq. (13), with $M/b_0 = 0.1$, $n = 1$ (first overtone) and $\ell = 0$, 1, 5 using the CFM.
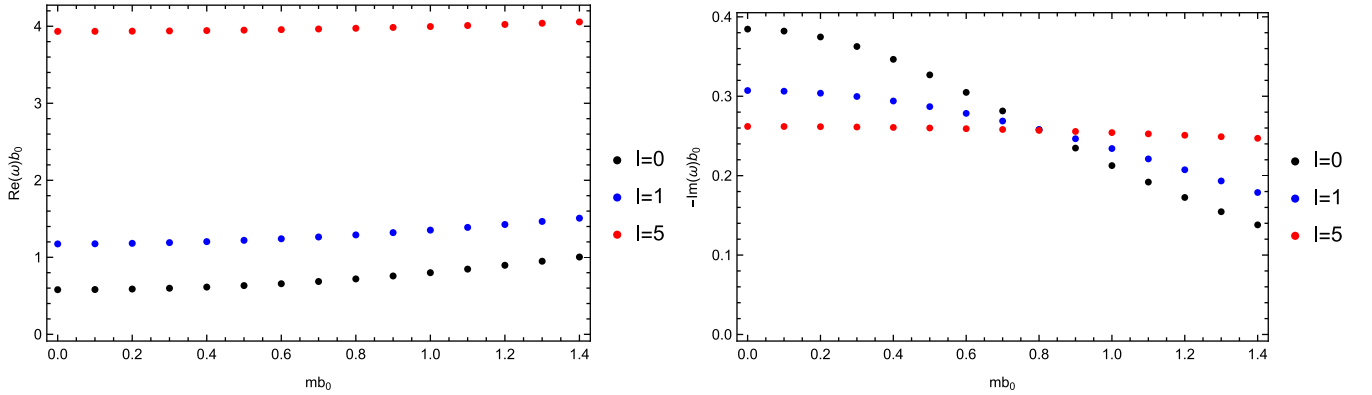
FIG. 6. The behavior of $\mathrm{Re}(\omega)b_0$ and $-\mathrm{Im}(\omega)b_0$ for a massive scalar field as a function of mb_0 for the wormhole spacetime described by Eq. (13), with $M/b_0 = 0.25$, $n = 0$ (fundamental frequency) and $\ell = 0$, 1, 5 using the CFM.
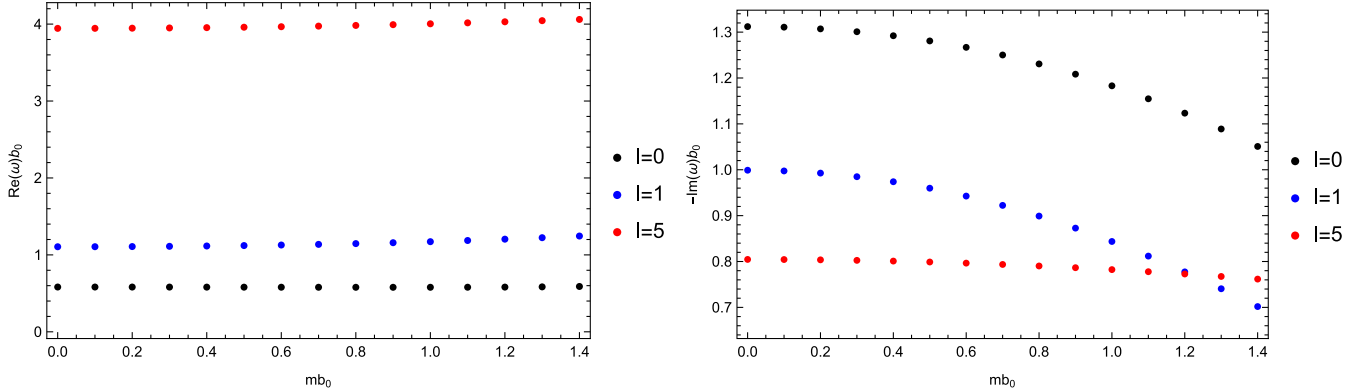
FIG. 7. The behavior of $\mathrm{Re}(\omega)b_0$ and $-\mathrm{Im}(\omega)b_0$ for a massive scalar field as a function of mb_0 for the wormhole spacetime described by Eq. (13), with $M/b_0 = 0.25$, $n = 1$ (first overtone) and $\ell = 0$, 1, 5 using the CFM.

B. Bound states

In this section we utilize the CFM to compute the bound states of massive scalar fields around the wormhole geometries defined in (13). These bound states are made feasible by the effective potential, which permits the existence of potential wells for $M \neq 0$, see Fig. 1. It is worth to mention

that the boundary conditions are different to that of QNMs. In this case we must considering evanescent waves at spatial infinity; therefore, the radial solution that satisfied the boundary condition at infinity is given by

$$u \sim e^{-\Omega r} r^{M\omega^2/\Omega} \quad \text{as } r \to \infty, \tag{30}$$

where $\Omega = \sqrt{m^2 - \omega^2}$. Generally, in a quantum system with a potential well, there are only a few bound states, the number of which depends on the potential parameters. In several cases, there exists only a single bound state. Thus, we just consider the first bound state which is described by the symmetric solution. Therefore, we consider the following ansatz for the solution to the radial equation (22) which satisfies the desired boundaries conditions

$$u(r) = e^{-\Omega r} r^{M\omega^2/\Omega} \sum_{n=0}^{\infty} a_n \left(\frac{r - b_0}{r} \right)^n. \quad (31)$$

Then, substituting this expression in the radial equation, the following seven-term recurrence relation is satisfied by the expansion coefficients:

$$c_0(0)a_1 + c_1(0)a_0 = 0,$$
$$c_0(1)a_2 + c_1(1)a_1 + c_2(1)a_0 = 0,$$
$$c_0(2)a_3 + c_1(2)a_2 + c_2(2)a_1 + c_3(2)a_0 = 0,$$
$$c_0(3)a_4 + c_1(3)a_3 + c_2(3)a_2 + c_3(3)a_1 + c_4(3)a_0 = 0,$$
$$c_0(4)a_5 + c_1(4)a_4 + c_2(4)a_3 + c_3(4)a_2 + c_4(4)a_1 + c_5(4)a_0 = 0,$$
$$c_0(n)a_{n+1} + c_1(n)a_n + c_2(n)a_{n-1} + c_3(n)a_{n-2} + c_4(n)a_{n-3} + c_5(n)a_{n-4} + c_6(n)a_{n-5} = 0, \quad n \geq 5, \quad (32)$$

where

$$c_0(n) = (n+1)(2n+1)(b_0 - 2M)(m^2 - \omega^2),$$

$$c_1(n) = b_0 \Big(\omega^2 \big(\ell^2 + \ell - 4Mn\sqrt{m^2 - \omega^2} - M\sqrt{m^2 - \omega^2} + 9n^2 + 1 \big) - m^2 (\ell^2 + \ell - 8Mn\sqrt{m^2 - \omega^2} - 2M\sqrt{m^2 - \omega^2}$$
$$+ 9n^2 + 1) \Big) - b_0^2 (m^2 - \omega^2)((4n+1)\sqrt{(m-\omega)(m+\omega)} - 2m^2 M) + b_0^3 (-(m^2 - \omega^2)^2) + 2M \Big((\ell^2 + \ell$$
$$+ 11n^2 + 1)(m^2 - \omega^2) - 4Mn\omega^2 \sqrt{m^2 - \omega^2} - M\omega^2 \sqrt{m^2 - \omega^2} \Big),$$

$$c_2(n) = 2b_0 \Big(m^2 \big(\ell^2 + \ell + 2n \big(-7M\sqrt{m^2 - \omega^2} + 4n - 6 \big) + 9M\sqrt{m^2 - \omega^2} + 4M^2\omega^2 + 6 \big) - \omega^2 \big(\ell^2 + \ell$$
$$+ n \big(-7M\sqrt{m^2 - \omega^2} + 8n - 12 \big) + 5M\sqrt{m^2 - \omega^2} + 3M^2\omega^2 + 6 \big) \Big) + b_0^2 (m^2 - \omega^2) \Big((10n - 7)$$
$$\sqrt{(m-\omega)(m+\omega)} - 6m^2 M \Big) + 2b_0^3 (m^2 - \omega^2)^2 + M(-(6\ell(\ell+1) + 25n(2n-3) + 37)(m^2 - \omega^2)$$
$$+ 36Mn\omega^2 \sqrt{m^2 - \omega^2} - 20M\omega^2 \sqrt{m^2 - \omega^2} - 4M^2\omega^4 \Big),$$

$$c_3(n) = b_0 \Big(\omega^2 \big(\ell^2 + \ell + 2n \big(-9M\sqrt{m^2 - \omega^2} + 7n - 21 \big) + 15M \big(2\sqrt{m^2 - \omega^2} + M\omega^2 \big) + 34 \big) - m^2 \big(\ell^2 + \ell$$
$$- 6n \big(6M\sqrt{m^2 - \omega^2} + 7 \big) + 55M\sqrt{m^2 - \omega^2} + 20M^2\omega^2 + 14n^2 + 34 \big) \Big) + b_0^2 (m^2 - \omega^2) \big(6m^2 M + (13 - 8n)$$
$$\sqrt{(m-\omega)(m+\omega)} \big) + b_0^3 (-(m^2 - \omega^2)^2) + M \Big(3(2\ell(\ell+1) + 20(n-3)n + 49)(m^2 - \omega^2)$$
$$- 64Mn\omega^2 \sqrt{m^2 - \omega^2} + 87M\omega^2 \sqrt{m^2 - \omega^2} + 14M^2\omega^4 \Big),$$

$$c_4(n) = b_0 \Big(m^2 \big(n \big(-20M\sqrt{m^2 - \omega^2} + 6n - 27 \big) + 16M \big(3\sqrt{m^2 - \omega^2} + M\omega^2 \big) + 31 \big) - \omega^2 \big(n \big(-10M\sqrt{m^2 - \omega^2}$$
$$+ 6n - 27 \big) + 26M\sqrt{m^2 - \omega^2} + 12M^2\omega^2 + 31 \big) \Big) + b_0^2 (m^2 - \omega^2) \big((2n-5)\sqrt{(m-\omega)(m+\omega)} - 2m^2 M \big)$$
$$+ M \big(-(2\ell(\ell+1) + 20n(2n-9) + 209)(m^2 - \omega^2) + 56Mn\omega^2 \sqrt{m^2 - \omega^2} - 121M\omega^2 \sqrt{m^2 - \omega^2} - 18M^2\omega^4 \big),$$

$$c_5(n) = b_0\Big(\omega^2\Big(n\Big(-2M\sqrt{m^2-\omega^2}+n-6\Big)+7M\sqrt{m^2-\omega^2}+3M^2\omega^2+9\Big) - m^2\Big(n\Big(-4M\sqrt{m^2-\omega^2}+n-6\Big)$$
$$+13M\sqrt{m^2-\omega^2}+4M^2\omega^2+9\Big)\Big) + M\Big(-24Mn\omega^2\sqrt{m^2-\omega^2}+71M\omega^2\sqrt{m^2-\omega^2}+(14(n-6)n+127)$$
$$(m^2-\omega^2)+10M^2\omega^4\Big),$$

$$c_6(n) = M\Big(\omega^2\Big(n\Big(4M\sqrt{m^2-\omega^2}+2n-15\Big)-15M\sqrt{m^2-\omega^2}-2M^2\omega^2+28\Big) - m^2(n-4)(2n-7)\Big).$$

Then, after applying Gaussian elimination four times, the original seven-term recurrence relations (32) can be simplified to a three-term relation, taking on the following concise form

$$\alpha_0 a_1 + \beta_0 a_0 = 0,$$
$$\alpha_n a_{n+1} + \beta_n a_n + \gamma_n a_{n-1} = 0, \quad n = 1, 2, \dots$$

We skip providing the explicit expressions for α_n, β_n and γ_n of the final three-term recurrence relations.

Now, according to Leaver [69,70], the recursion coefficients must satisfy the following continued fraction relation for the convergence of the series

$$\beta_0 - \frac{\alpha_0\gamma_1}{\beta_1-}\frac{\alpha_1\gamma_2}{\beta_2-}\cdots\frac{\alpha_n\gamma_{n+1}}{\beta_{n+1}-}\cdots = 0, \qquad (33)$$

and the continued fraction must be truncated at some large index N. The bound states frequencies are obtained solving this equation numerically. In Tables I and II, we show some values of the lowest bound states frequencies ωb_0 for scalar perturbations using the CFM. We observe that the oscillation frequency increases when the mass parameter $m b_0$ increases and when the angular number ℓ increases.

V. $f(R)$ GRAVITY WORMHOLE

In the framework of $f(R)$ modified gravity, a generalization of the Ellis drainhole solution was found in [65] by considering a phantom scalar field with a self-interacting potential. The solution is given by

$$\Phi(r) = 0, \qquad b(r) = 2r - \mu^2 r^3,$$
$$\phi(r) = \sqrt{6}\frac{\sqrt{A}}{r}, \qquad V(\phi) = \frac{1}{2}\mu^2\phi^2. \qquad (34)$$

The condition $\frac{b(r)}{r} \le 1$ reduces to $\mu^2 r^2 \ge 1$, which holds for all r within the interval $[\frac{1}{\mu}, +\infty)$. Also, the condition $\frac{b(r)}{r} = 1$ yields the throat location at $r_{\text{th}} = \frac{1}{\mu}$, where μ can be interpreted as the mass of the phantom scalar field. Furthermore, the flare-out condition $b'(r) < \frac{b(r)}{r}$ results in $\mu^2 r^2 > 0$, which is satisfied for every $r > 0$ and $\mu \ne 0$. Also, it can be easily verified that $b'(r_{\text{th}}) = -1$, ensuring that the relation $b'(r_{\text{th}}) \le 1$ always holds true.

The fundamental characteristics of the solution highlight the impact of the phantom scalar field on both the scalar curvature and the throat's size. As the strength of the scalar field intensifies, the resulting wormholes exhibit larger throat radii, consequently diminishing the curvature in the vicinity of the throat. We direct the reader to Ref. [65] for a comprehensive review of the solution.

A. Analytical QNFs of $f(R)$ gravity wormhole

In this section we study the propagation of a probe scalar field in the $f(R)$ wormhole geometry, with a particular focus on studying its stability through the QNFs. In this case the Klein-Gordon equation, considering the following separation of variables

$$\Psi(t, r, \theta, \varphi) = e^{-i\omega t}\frac{u(r)}{r}Y_\ell(\Omega), \qquad (35)$$

TABLE I. Frequencies (ωb_0) of the lowest bound states for scalar perturbations in the wormhole spacetime described by Eq. (13), with $M/b_0 = 0.1$, $\ell = 0, 1$, and several values of the scalar field mass using the CFM.

ℓ	$mb_0 = 0.4$	$mb_0 = 0.8$	$mb_0 = 1.2$	$mb_0 = 1.6$
0	0.39967670	0.79727718	1.18979435	1.57334204
1	0.39991988	0.79935626	1.19781061	1.59474718

ℓ	$mb_0 = 2$	$mb_0 = 2.4$	$mb_0 = 2.8$	$mb_0 = 3.2$
0	1.94709369	2.31390013	2.67665885	3.03714485
1	1.98954025	2.38132146	2.76858541	3.14873064

TABLE II. Frequencies (ωb_0) of the lowest bound states for scalar perturbations in the wormhole spacetime described by Eq. (13), with $M/b_0 = 0.25$, $\ell = 0, 1$ and several values of the scalar field mass using the CFM.

ℓ	$mb_0 = 0.4$	$mb_0 = 0.8$	$mb_0 = 1.2$	$mb_0 = 1.6$
0	0.39948020	0.77659459	1.10626752	1.40450402
1	0.39949541	0.79583960	1.18498187	1.55693415

ℓ	$mb_0 = 2$	$mb_0 = 2.4$	$mb_0 = 2.8$	$mb_0 = 3.2$
0	1.69213119	1.97599183	2.25838693	2.54020128
1	1.87946685	2.16141735	2.43284661	2.70240221

can be written as a one-dimensional Schrödinger-like equation

$$\frac{d^2u}{dr^{*2}} + [\omega^2 - V(r^*)]u = 0, \tag{36}$$

where ω is the unknown frequency, while $Y_\ell(\Omega)$ are the spherical harmonics and r^* is the well-known tortoise coordinate, i.e.,

$$r^* \equiv \int \frac{dr}{e^\Phi \sqrt{1 - \frac{b(r)}{r}}}. \tag{37}$$

The effective potential governing scalar perturbations for the $f(R)$ gravity wormhole reads

$$V(r) = \frac{\ell(\ell+1)}{r^2} + \mu^2 + m^2, \tag{38}$$

which is plotted in Fig. 8. We observe that the effective potential is symmetric about the throat of the wormhole and takes the form of a barrier for $\ell \neq 0$, with the barrier magnitude increasing with ℓ. However, it does not allow wells, consequently precluding the support for bound states.

It is worth noticing that when $\ell = 0$ the effective potential is constant. Consequently, the solution of the radial function is given by $u = C_1 e^{i\sqrt{\omega^2-\mu^2-m^2}r^*} + C_2 e^{-i\sqrt{\omega^2-\mu^2-m^2}r^*}$. Imposing the condition of purely
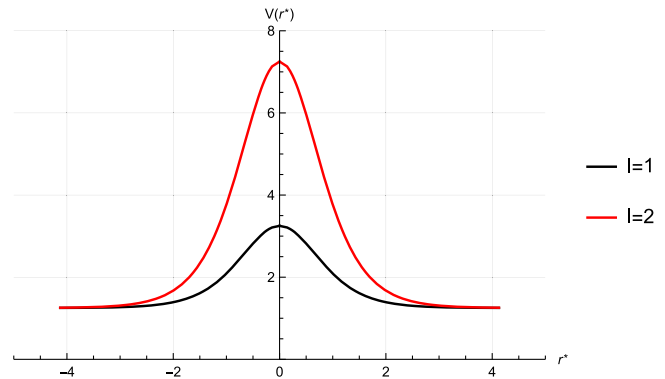
FIG. 8. Effective potential for $\mu = 1$, $m = 0.5$ and $\ell = 1, 2$.

outgoing waves at both infinities leads to the conclusion that $C_1 = C_2 = 0$, resulting in $u = 0$ for this particular case.

Now we consider the case $\ell \neq 0$. The radial equation can be written as

$$(1 - \tilde{r}^2)\frac{d^2}{d\tilde{r}^2}u(\tilde{r}) - \tilde{r}\frac{d}{d\tilde{r}}u(\tilde{r})$$
$$+ \left(\frac{\ell(\ell+1)}{\tilde{r}^2} - \tilde{\omega}^2 + 1 + \tilde{m}^2\right)u(\tilde{r}) = 0, \tag{39}$$

where we have defined a dimensionless coordinate $\tilde{r} = \mu r$, $\tilde{m} = m/\mu$ and $\tilde{\omega} = \omega/\mu$. The radial equation can be analytically solved by expressing it in terms of hypergeometric functions

$$u(\tilde{r}) = C_1 \tilde{r}^{\frac{1}{2}(1-\sqrt{1-4\ell(\ell+1)})} {}_2F_1\left(\frac{1}{4} - \frac{1}{4}\sqrt{1-4\ell(\ell+1)} - \frac{\sqrt{1+\tilde{m}^2-\tilde{\omega}^2}}{2}, \frac{1}{4} - \frac{1}{4}\sqrt{1-4\ell(\ell+1)} + \frac{\sqrt{1+\tilde{m}^2-\tilde{\omega}^2}}{2}, \right.$$
$$\left. 1 - \frac{1}{2}\sqrt{1-4\ell(\ell+1)}, \tilde{r}^2\right) + C_2 r^{\frac{1}{2}(1+\sqrt{1-4\ell(\ell+1)})} {}_2F_1\left(\frac{1}{4} + \frac{1}{4}\sqrt{1-4\ell(\ell+1)} - \frac{\sqrt{1+\tilde{m}^2-\tilde{\omega}^2}}{2}, \right.$$
$$\left. \frac{1}{4} + \frac{1}{4}\sqrt{1-4\ell(\ell+1)} + \frac{\sqrt{1+\tilde{m}^2-\tilde{\omega}^2}}{2}, 1 + \frac{1}{2}\sqrt{1-4\ell(\ell+1)}, \tilde{r}^2\right), \tag{40}$$

where ${}_2F_1$ is the Gaussian hypergeometric function.

Since the potential is symmetric about the throat of the wormhole, which is located at $r_0^* = 0$, the solutions will be symmetric or antisymmetric. Therefore, we impose the following boundary conditions at the throat, $\frac{du}{dr^*}|_{r_0^*} = 0$ for the symmetric solutions and $u(r_0^*) = 0$ for the antisymmetric solutions. These boundary conditions yields the even and odd overtones, respectively. For the symmetric solutions the condition at the throat $\frac{du}{dr^*}|_{r_0^*} = \frac{du}{d\tilde{r}}\sqrt{1 - \frac{b(\tilde{r})}{\tilde{r}}}|_{\tilde{r}=1} = 0$ yields

$$C_1 = C_2\rho\frac{\Gamma[1+\alpha_+]\Gamma[1+\alpha_-]\Gamma[1+\frac{1}{2}\sqrt{1-4\ell(\ell+1)}]}{\Gamma[1+\gamma_-]\Gamma[1+\gamma_+]\Gamma[1-\frac{1}{2}\sqrt{1-4\ell(\ell+1)}]},$$

where

$$\rho = \frac{-2(2-\sqrt{1-4\ell(\ell+1)})\tilde{m}^2 - 3 + 4\tilde{\omega}^2 + \sqrt{1-4\ell(\ell+1)}((3+2\ell(\ell+1)) - 2\tilde{\omega}^2)}{(2\tilde{m}^2 + (1+2\ell(\ell+1) + \sqrt{1-4\ell(\ell+1)}) - 2\tilde{\omega}^2)(2-\sqrt{1-4\ell(\ell+1)})},$$

and the asymptotic behavior of the solutions is

$$
u(\tilde{r}) \sim C_2 \tilde{r}^{-i\sqrt{\tilde{\omega}^2 - 1 - \tilde{m}^2}} \Gamma[-\sqrt{1 + \tilde{m}^2 - \tilde{\omega}^2}] \Gamma\left[1 + \frac{1}{2}\sqrt{1 - 4\ell(\ell+1)}\right] \left((-1)^{-\alpha_+} \rho(\alpha_-/\gamma_-) \frac{\Gamma[1 + \alpha_+]}{\Gamma[\beta_-]\Gamma[1 + \gamma_+]}\right.
$$
$$
\left. + \frac{(-1)^{-\gamma_+}}{\Gamma[\delta_-]}\right) \frac{1}{\Gamma[\gamma_-]} + C_2 \tilde{r}^{i\sqrt{\tilde{\omega}^2 - 1 - \tilde{m}^2}} \Gamma[\sqrt{1 + \tilde{m}^2 - \tilde{\omega}^2}] \Gamma\left[1 + \frac{1}{2}\sqrt{1 - 4\ell(\ell+1)}\right]
$$
$$
\left((-1)^{-\alpha_-} \rho(\alpha_+/\gamma_+) \frac{\Gamma[1 + \alpha_-]}{\Gamma[\beta_+]\Gamma[1 + \gamma_-]} + \frac{(-1)^{-\gamma_-}}{\Gamma[\delta_+]}\right) \frac{1}{\Gamma[\gamma_+]}, \tag{41}
$$

where we have defined

$$
\alpha_\pm = \frac{1}{4} - \frac{\sqrt{1 - 4\ell(\ell+1)}}{4} \pm \frac{\sqrt{1 + \tilde{m}^2 - \tilde{\omega}^2}}{2}, \qquad \beta_\pm = \frac{3}{4} - \frac{\sqrt{1 - 4\ell(\ell+1)}}{4} \pm \frac{\sqrt{1 + \tilde{m}^2 - \tilde{\omega}^2}}{2},
$$
$$
\gamma_\pm = \frac{1}{4} + \frac{\sqrt{1 - 4\ell(\ell+1)}}{4} \pm \frac{\sqrt{1 + \tilde{m}^2 - \tilde{\omega}^2}}{2}, \qquad \delta_\pm = \frac{3}{4} + \frac{\sqrt{1 - 4\ell(\ell+1)}}{4} \pm \frac{\sqrt{1 + \tilde{m}^2 - \tilde{\omega}^2}}{2}.
$$

Now, in accordance with the boundary condition of purely outgoing waves at spatial infinity, i.e. $u \sim r^{i\sqrt{\tilde{\omega}^2 - 1 - \tilde{m}^2}}$, we set

$$
\gamma_- = \frac{1}{4} + \frac{\sqrt{1 - 4\ell(\ell+1)}}{4} - \frac{\sqrt{1 + \tilde{m}^2 - \tilde{\omega}^2}}{2} = -n \qquad n = 0, 1, \ldots \tag{42}
$$

Therefore, the QNFs for even overtones yield

$$
\tilde{\omega} = \frac{1}{\sqrt{2}}\left(\eta + \left(\eta^2 + \frac{1}{4}(-1 + 4\ell(\ell+1))(1 + 4n)^2\right)^{1/2}\right)^{1/2} - i\frac{(-1 + 4\ell(\ell+1))^{1/2}(1 + 4n)}{2\sqrt{2}(\eta + (\eta^2 + \frac{1}{4}(-1 + 4\ell(\ell+1))(1 + 4n)^2)^{1/2})^{1/2}}, \tag{43}
$$

where $\eta \equiv \frac{1}{2}(1 + 2\ell(\ell+1) - 4n(1 + 2n)) + \tilde{m}^2$.

On the other hand, the boundary condition at the throat $u(1) = 0$ for the antisymmetric solutions leads to the expression

$$
C_1 = -C_2 \frac{\Gamma[\beta_+]\Gamma[\beta_-]\Gamma[1 + \frac{1}{2}\sqrt{1 - 4\ell(\ell+1)}]}{\Gamma[\gamma_+]\Gamma[\gamma_-]\Gamma[1 - \frac{1}{2}\sqrt{1 - 4\ell(\ell+1)}]}.
$$

Thus, the asymptotic behavior of the solutions is

$$
u(\tilde{r}) \sim C_2 \tilde{r}^{-i\sqrt{\tilde{\omega}^2 - 1 - \tilde{m}^2}} \Gamma[-\sqrt{1 + \tilde{m}^2 - \tilde{\omega}^2}] \Gamma\left[1 + \frac{1}{2}\sqrt{1 - 4\ell(\ell+1)}\right]\left(-(-1)^{-\alpha_+} \frac{\Gamma[\beta_+]}{\Gamma[\alpha_-]\Gamma[\delta_+]} + \frac{(-1)^{-\gamma_+}}{\Gamma[\gamma_-]}\right) \frac{1}{\Gamma[\delta_-]}
$$
$$
+ C_2 \tilde{r}^{i\sqrt{\tilde{\omega}^2 - 1 - \tilde{m}^2}} \Gamma[\sqrt{1 + \tilde{m}^2 - \tilde{\omega}^2}] \Gamma\left[1 + \frac{1}{2}\sqrt{1 - 4\ell(\ell+1)}\right]\left(-(-1)^{-\alpha_-} \frac{\Gamma[\beta_-]}{\Gamma[\alpha_+]\Gamma[\delta_-]} + \frac{(-1)^{-\gamma_-}}{\Gamma[\gamma_+]}\right) \frac{1}{\Gamma[\delta_+]}. \tag{44}
$$

Now, in accordance with the boundary condition of purely outgoing waves at spatial infinity, i.e. $u \sim r^{i\sqrt{\tilde{\omega}^2 - 1 - \tilde{m}^2}}$, we set

$$
\delta_- = \frac{3}{4} + \frac{\sqrt{1 - 4\ell(\ell+1)}}{4} - \frac{\sqrt{1 + \tilde{m}^2 - \tilde{\omega}^2}}{2} = -n \quad n = 0, 1, \ldots \tag{45}
$$

and the QNFs for odd overtones yield

$$
\tilde{\omega} = \frac{1}{\sqrt{2}}\left(\eta' + \left(\eta'^2 + \frac{1}{4}(-1 + 4\ell(\ell+1))(3 + 4n)^2\right)^{1/2}\right)^{1/2} - i\frac{(-1 + 4\ell(\ell+1))^{1/2}(3 + 4n)}{2\sqrt{2}(\eta' + (\eta'^2 + \frac{1}{4}(-1 + 4\ell(\ell+1))(3 + 4n)^2)^{1/2})^{1/2}}, \tag{46}
$$

where $\eta' \equiv \frac{1}{2}(-3 + 2\ell(\ell+1) - 4n(3 + 2n)) + \tilde{m}^2$.

Finally, the QNFs given by Eq. (43) for even overtones and Eq. (46) for odd overtones can be succinctly expressed in a unified formula as

$$\tilde{\omega} = \frac{1}{\sqrt{2}}\left(\eta'' + \left(\eta''^2 + \frac{1}{4}(-1+4\ell(\ell+1))(1+2n)^2\right)^{1/2}\right)^{1/2} - i\frac{(-1+4\ell(\ell+1))^{1/2}(1+2n)}{2\sqrt{2}(\eta''+(\eta''^2+\frac{1}{4}(-1+4\ell(\ell+1))(1+2n)^2)^{1/2})^{1/2}}, \quad (47)$$

where $\eta'' \equiv \frac{1}{2}(1 + 2\ell(\ell+1) - 2n(1+n)) + \tilde{m}^2$ and $n = 0, 1, \ldots$. In Figs. 9 and 10 we plot the behavior of $\text{Re}(\tilde{\omega})$ and $-\text{Im}(\tilde{\omega})$ as a function of $\tilde{m}$ by using the analytical expression (47) for $n = 0$ and $n = 1$, respectively. We can observe that the modes with the lowest angular number ℓ exhibit the longest lifetimes, both for the fundamental and the first overtone, and the decay rate decreases with $\tilde{m}$. Additionally, the frequency of oscillation increases with higher values of the parameter $\tilde{m}$ and the angular momentum ℓ.

All the frequencies exhibit a negative imaginary part, indicating the stability of the propagation of massive scalar fields in this background. Defining $L = \sqrt{\ell(\ell+1)}$ and considering high values of L, this expression can be approximated to

$$\tilde{\omega} \approx L + \frac{3+4\tilde{m}^2}{8L} - i\left(\frac{1}{2} + n - \frac{(1+\tilde{m}^2)(1+2n)}{4L^2}\right). \quad (48)$$

As we will see in the next subsection this result match with the QNFs obtained via the third order WKB method.

B. WKB method

In this section, we employ the WKB approximation method, first introduced by Mashhoon [80] and later developed by Schutz and Iyer [81], to obtain the QNFs. This approach allows us to gain insights into the behavior of QNFs in the eikonal limit as $\ell \to \infty$. Our aim is to validate and complement the analytical results obtained in the previous section using an alternative method. Iyer and Will computed the third order correction [82], which was
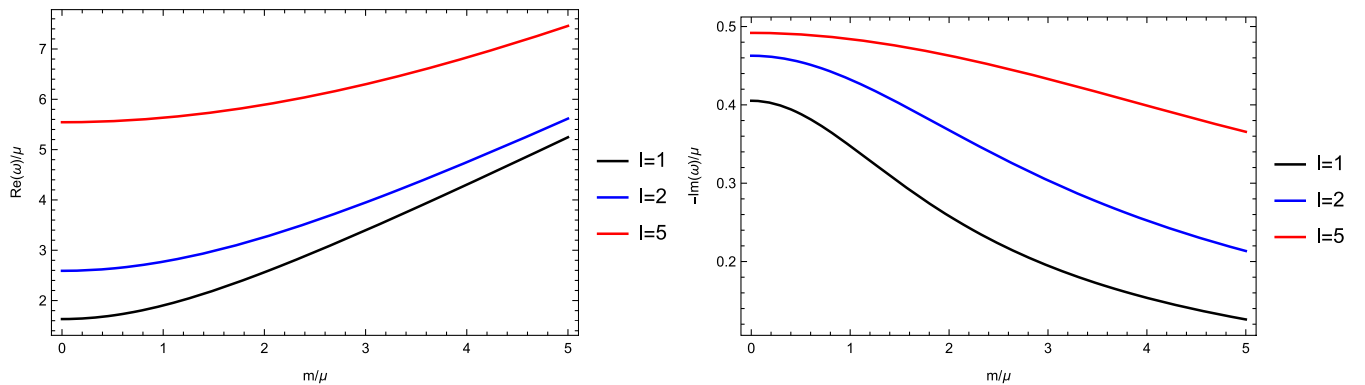
FIG. 9.   The behavior of $\text{Re}(\omega)/\mu$ (left panel) and $-\text{Im}(\omega)/\mu$ (right panel) as a function of m/μ for different values of ℓ and $n = 0$.
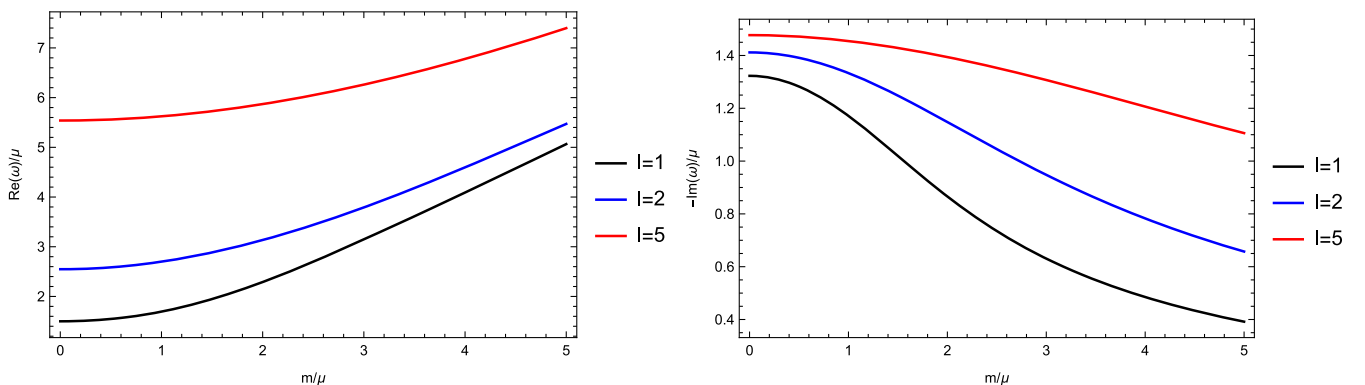
FIG. 10.   The behavior of $\text{Re}(\omega)/\mu$ (left panel) and $-\text{Im}(\omega)/\mu$ (right panel) as a function of m/μ for different values of ℓ and $n = 1$.

subsequently extended to the sixth order [83], and recently up to the 13th order [84], see also [85].

This method has been used to determine the QNFs for asymptotically flat and asymptotically de Sitter black holes. This is due to the WKB method can be used for effective potentials which have the form of potential barriers that approach to a constant value at the horizon and spatial infinity [37]. The QNMs are determined by the behavior of the effective potential near its maximum value $V(r^*_{max})$. The Taylor series expansion of the potential around its maximum is given by

$$V(r^*) = V(r^*_{max}) + \sum_{i=2}^{\infty} \frac{V^{(i)}}{i!} (r^* - r^*_{max})^i, \quad (49)$$

where

$$V^{(i)} = \frac{d^i}{dr^{*i}} V(r^*)\big|_{r^* = r^*_{max}}, \quad (50)$$

corresponds to the ith derivative of the potential with respect to r^* evaluated at the position of the maximum of the potential r^*_{max}. Using the WKB approximation up to third order beyond the eikonal limit, the QNFs are given by the following expression [86]

$$\omega^2 = V(r^*_{max}) - 2iU, \quad (51)$$

where

$$U = N\sqrt{-V^{(2)}/2} + \frac{i}{64}\left(-\frac{1}{9}\frac{V^{(3)2}}{V^{(2)2}}(7 + 60N^2) + \frac{V^{(4)}}{V^{(2)}}(1 + 4N^2)\right) + \frac{N}{2^{3/2}288}\left(\frac{5}{24}\frac{V^{(3)4}}{(-V^{(2)})^{9/2}}(77 + 188N^2)\right.$$
$$\left. + \frac{3}{4}\frac{V^{(3)2}V^{(4)}}{(-V^{(2)})^{7/2}}(51 + 100N^2) + \frac{1}{8}\frac{V^{(4)2}}{(-V^{(2)})^{5/2}}(67 + 68N^2) + \frac{V^{(3)}V^{(5)}}{(-V^{(2)})^{5/2}}(19 + 28N^2) + \frac{V^{(6)}}{(-V^{(2)})^{3/2}}(5 + 4N^2)\right),$$

and $N = n + 1/2$, with $n = 0, 1, 2, \ldots$, is the overtone number. Now, defining $L^2 = \ell(\ell + 1)$, we find that for large values of L, the QNFs are approximately given by

$$\tilde{\omega} \approx \omega_1 L + \omega_0 + \omega_{-1}L^{-1} + \omega_2 L^{-2} + \mathcal{O}(L^{-3}). \quad (52)$$

The maximum of the potential is located at the throat $\tilde{r} = 1$ and its value is given by

$$V(r^*_0) = L^2 + 1 + \tilde{m}^2, \quad (53)$$

and the derivatives of the potential are

$$V^{(2)}(r^*_0) = -2L^2, \quad V^{(3)}(r^*_0) = 0, \quad V^{(4)}(r^*_0) = 16L^2,$$
$$V^{(5)}(r^*_0) = 0, \quad V^{(6)}(r^*_0) = -272L^2. \quad (54)$$

Therefore, the QNFs for large L are approximately given by

$$\tilde{\omega} \approx L + \frac{3 + 4\tilde{m}^2}{8L} - i\left(\frac{1}{2} + n - \frac{(1 + \tilde{m}^2)(1 + 2n)}{4L^2}\right). \quad (55)$$

This result, as previously mentioned, coincides with the earlier finding, as shown in Eq. (48). Now, we plot the behavior of $\mathrm{Re}(\omega)/\mu$, and $-\mathrm{Im}(\omega/\mu)$ as a function of m/μ by using the sixth order WKB method for $n = 0$ (see Fig. 11) and $n = 1$ (see Fig. 12). We can observe that the modes with the lowest angular number ℓ exhibit the longest lifetimes, both for the fundamental and the first overtone. Additionally, the frequency of oscillation increases with higher values of the parameter m/μ and angular momentum ℓ. Therefore, in this wormhole geometry the anomalous decay of QNFs is avoided.
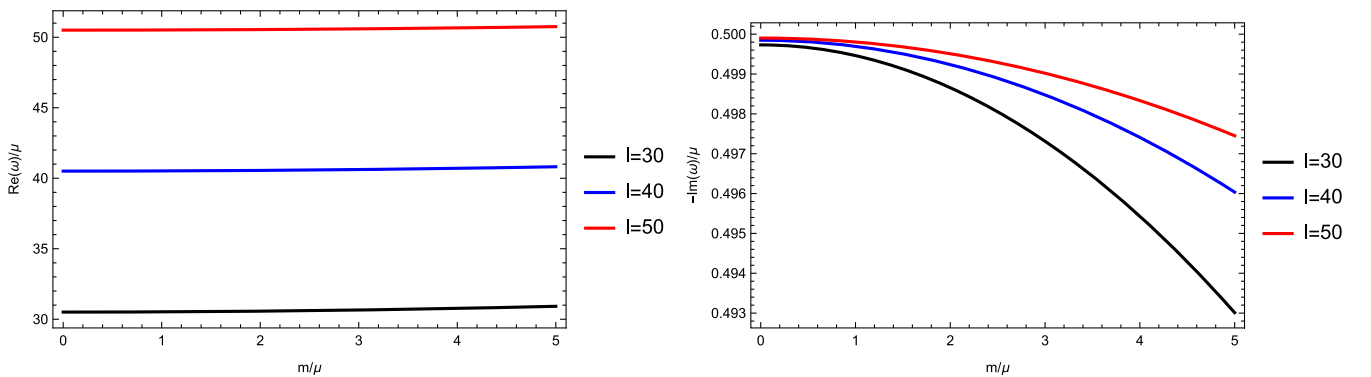
FIG. 11.   The behavior of $\mathrm{Re}(\omega)/\mu$ (left panel) and $-\mathrm{Im}(\omega)/\mu$ (right panel) as a function of m/μ for different values of ℓ using the six order WKB method and $n = 0$.
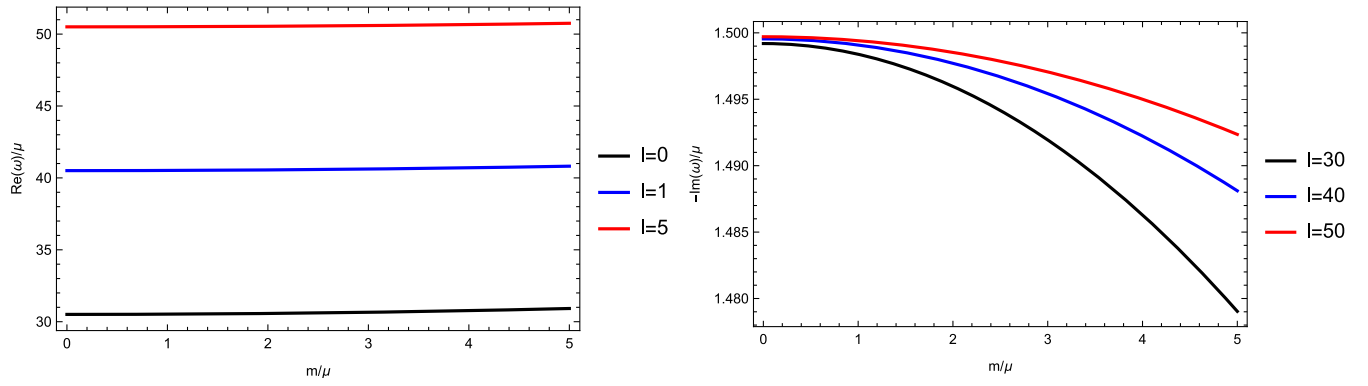
FIG. 12. The behavior of $\text{Re}(\omega)/\mu$ (left panel) and $-\text{Im}(\omega)/\mu$ (right panel) as a function of m/μ for different values of ℓ using the sixth order WKB method and $n = 1$.

VI. CONCLUSIONS

In this work, we explored wormhole geometries with a nonconstant redshift function by introducing a gravitational mass M, which goes over into the Bronnikov-Ellis wormhole when the gravitational mass parameter vanishes and an $f(R)$ gravity wormhole spacetime as background geometries and investigated the propagation of massive scalar fields.

For the wormholes with a nonconstant reshift function, our analysis focused primarily on low values of the angular number ℓ, and we determined the QNFs using the CFM. These QNFs exhibit an inverted behavior of $\text{Im}(\omega)b_0$: when $mb_0 > m_c b_0$, $\text{Im}(\omega)b_0$ increases with ℓ, representing an anomalous decay rate of the QNMs. Conversely, for $mb_0 < m_c b_0$, $\text{Im}(\omega)b_0$ decreases with increasing ℓ for $n \geq \ell$. The critical value $m_c b_0$ rises with an increase in the parameter M/b_0, and the frequency of the oscillation increases with both the angular number and the parameter mb_0. Additionally, for the geometries with $M \neq 0$ we identified bound states characterized by an oscillation frequency without decay that rises with increasing mb_0 and ℓ. On the other hand, for $M = 0$ the effective potential does not forms wells, and bound states are prohibited in this case.

Then, we considered a wormhole spacetime that is an exact solution of $f(R)$ modified gravity with a phantom scalar field with a self-interacting potential. We obtained exact results for the QNFs, which, for large values of ℓ, coincide with the third-order WKB approximation. Here, the longest-lived modes are those with the lowest angular

number ℓ, both for the fundamental and the first overtone. Furthermore, the oscillation frequency increases with a rise in the parameter m/μ and angular momentum ℓ. Thus, in this wormhole background, the anomalous behavior observed in the first spacetimes is avoided. Also, the effective potential is symmetric about the throat of the wormhole and it does not allow wells, consequently bound states are not supported in this wormhole spacetime.

The analysis of the wormholes considered reveals that those with a constant redshift function do not support bound states, in contrast to those with a nonconstant redshift function (resulting in a nonzero tidal radial force), which do permit bound states.

ACKNOWLEDGMENTS

APPENDIX A: NUMERICAL VALUES

In this appendix we provide some numerical values of the QNFs via CFM for the wormhole spacetime described by Eq. (13). In Tables III, IV, and V we show the QNFs for the fundamental mode for $M/b_0 = 0$, $M/b_0 = 0.1$, and $M/b_0 = 0.25$, respectively, and in Tables VI, VII, and VIII we show the QNFs for the first overtone ($n = 1$) for $M/b_0 = 0$, $M/b_0 = 0.1$, and $M/b_0 = 0.25$, respectively.

TABLE III. Fundamental $n = 0$ QNFs ωb_0 for scalar perturbations for the Bronnikov-Ellis wormhole for several values of the angular momentum and the mass of the scalar field using the CFM.

ℓ	$mb_0 = 0$	$mb_0 = 0.2$	$mb_0 = 0.4$	$mb_0 = 0.6$
0	$0.68136719 - 0.61775345\,i$	$0.69762539 - 0.60335666\,i$	$0.74791262 - 0.56278891\,i$	$0.83479189 - 0.50421780\,i$
1	$1.57270839 - 0.52970088\,i$	$1.58410509 - 0.52589000\,i$	$1.61799977 - 0.51487339\,i$	$1.67350804 - 0.49779565\,i$
2	$2.54665642 - 0.51266881\,i$	$2.55419456 - 0.51115579\,i$	$2.57669677 - 0.50669188\,i$	$2.61383299 - 0.49949302\,i$
3	$3.53428741 - 0.50692165\,i$	$3.53982819 - 0.50612818\,i$	$3.55640289 - 0.50376936\,i$	$3.58387030 - 0.49990838\,i$
5	$5.52230920 - 0.50295823\,i$	$5.52589995 - 0.50263141\,i$	$5.53665868 - 0.50165471\,i$	$5.55454509 - 0.50003931\,i$
10	$10.51183964 - 0.50083853\,i$	$10.51373778 - 0.50074811\,i$	$10.51943015 - 0.50047714\,i$	$10.52891067 - 0.50002650\,i$
15	$15.50804389 - 0.50038767\,i$	$15.50933215 - 0.50034610\,i$	$15.51319628 - 0.50022147\,i$	$15.51963438 - 0.50001396\,i$

ℓ	$mb_0 = 0.8$	$mb_0 = 1.0$	$mb_0 = 1.2$	$mb_0 = 1.4$
0	$0.95710482 - 0.43978143\,i$	$1.10771470 - 0.37998677\,i$	$1.27720491 - 0.32956100\,i$	$1.45807345 - 0.28868020\,i$
1	$1.74918582 - 0.47625873\,i$	$1.84312741 - 0.45198450\,i$	$1.95313933 - 0.42652616\,i$	$2.07694738 - 0.40110069\,i$
2	$2.66507432 - 0.48988928\,i$	$2.72972309 - 0.47828709\,i$	$2.80695095 - 0.46512795\,i$	$2.89584111 - 0.45085047\,i$
3	$3.62200113 - 0.49464557\,i$	$3.67048645 - 0.48811154\,i$	$3.72894874 - 0.48045895\,i$	$3.79695454 - 0.47185363\,i$
5	$5.57949282 - 0.49780347\,i$	$5.61141062 - 0.49497195\,i$	$5.65018391 - 0.49157531\,i$	$5.69567673 - 0.48764897\,i$
10	$10.54216920 - 0.49939763\,i$	$10.55919163 - 0.49859255\,i$	$10.57995997 - 0.49761382\,i$	$10.60445239 - 0.49646451\,i$
15	$15.52864326 - 0.49972388\,i$	$15.54021845 - 0.49935166\,i$	$15.55435426 - 0.49889785\,i$	$15.57104374 - 0.49836312\,i$

TABLE IV. Fundamental $n = 0$ QNFs ωb_0 for scalar perturbations for the wormhole spacetime described by Eq. (13) with $M/b_0 = 0.1$, for several values of the angular momentum and the mass of the scalar field using the CFM.

ℓ	$mb_0 = 0$	$mb_0 = 0.2$	$mb_0 = 0.4$	$mb_0 = 0.6$
0	$0.64217472 - 0.52979187\,i$	$0.65556756 - 0.51733481\,i$	$0.69692010 - 0.48206571\,i$	$0.76830083 - 0.43049763\,i$
1	$1.42443104 - 0.44987061\,i$	$1.43440781 - 0.44629804\,i$	$1.46408863 - 0.43594442\,i$	$1.51272479 - 0.41981413\,i$
2	$2.28995771 - 0.43248900\,i$	$2.29664353 - 0.43105279\,i$	$2.31660278 - 0.42681157\,i$	$2.34954643 - 0.41995908\,i$
3	$3.17040105 - 0.42628276\,i$	$3.17533511 - 0.42552688\,i$	$3.19009512 - 0.42327874\,i$	$3.21455621 - 0.41959546\,i$
5	$4.94550683 - 0.42182228\,i$	$4.94871268 - 0.42151025\,i$	$4.95831818 - 0.42057757\,i$	$4.97428747 - 0.41903441\,i$
10	$9.40544221 - 0.41934024\,i$	$9.40713911 - 0.41925382\,i$	$9.41222797 - 0.41899482\,i$	$9.42070336 - 0.41856403\,i$
15	$13.87311667 - 0.41879955\,i$	$13.87426865 - 0.41875982\,i$	$13.87772405 - 0.41864067\,i$	$13.88348113 - 0.41844227\,i$

ℓ	$mb_0 = 0.8$	$mb_0 = 1.0$	$mb_0 = 1.2$	$mb_0 = 1.4$
0	$0.86912831 - 0.37246044\,i$	$0.99422781 - 0.31703053\,i$	$1.13627138 - 0.26904009\,i$	$1.28910794 - 0.22942901\,i$
1	$1.57908796 - 0.39932068\,i$	$1.66154662 - 0.37599623\,i$	$1.75820800 - 0.35123892\,i$	$1.86709221 - 0.32616103\,i$
2	$2.39501097 - 0.41079193\,i$	$2.45238427 - 0.39967609\,i$	$2.52093849 - 0.38701017\,i$	$2.59986671 - 0.37319156\,i$
3	$3.24851550 - 0.41456774\,i$	$3.29169959 - 0.40831378\,i$	$3.34377421 - 0.40097186\,i$	$3.40435536 - 0.39269243\,i$
5	$4.99656144 - 0.41689732\,i$	$5.02505886 - 0.41418882\,i$	$5.05967769 - 0.41093663\,i$	$5.10029687 - 0.40717299\,i$
10	$9.43255622 - 0.41796278\,i$	$9.44777395 - 0.41719290\,i$	$9.46634048 - 0.41625671\,i$	$9.48823630 - 0.41515702\,i$
15	$13.89153706 - 0.41816492\,i$	$13.90188784 - 0.41780899\,i$	$13.91452839 - 0.41737499\,i$	$13.92945250 - 0.41686353\,i$

TABLE V. Fundamental $n = 0$ QNFs ωb_0 for scalar perturbations for the wormhole spacetime described by Eq. (13) with $M/b_0 = 0.25$, for several values of the angular momentum and the mass of the scalar field using the CFM.

ℓ	$mb_0 = 0$	$mb_0 = 0.2$	$mb_0 = 0.4$	$mb_0 = 0.6$
0	$0.57954862 - 0.38454705\,i$	$0.58788305 - 0.37466006\,i$	$0.61338274 - 0.34648046\,i$	$0.65699718 - 0.30486477\,i$
1	$1.17377910 - 0.30720290\,i$	$1.18130424 - 0.30383997\,i$	$1.20370378 - 0.29401135\,i$	$1.24044319 - 0.27843471\,i$
2	$1.84793711 - 0.28302527\,i$	$1.85314787 - 0.28162482\,i$	$1.86870696 - 0.27747445\,i$	$1.89439869 - 0.27072045\,i$
3	$2.53780145 - 0.27199629\,i$	$2.54168130 - 0.27124742\,i$	$2.55328871 - 0.26901575\,i$	$2.57252849 - 0.26534505\,i$
5	$3.93343488 - 0.26196975\,i$	$3.93596757 - 0.26165516\,i$	$3.94355629 - 0.26071402\,i$	$3.95617323 - 0.25915412\,i$
10	$7.45015539 - 0.25438498\,i$	$7.45149755 - 0.25429618\,i$	$7.45552258 - 0.25402996\,i$	$7.46222623 - 0.25358694\,i$
15	$10.97800980 - 0.25223172\,i$	$10.97892087 - 0.25219058\,i$	$10.98165362 - 0.25206720\,i$	$10.98620671 - 0.25186172\,i$

ℓ	$mb_0 = 0.8$	$mb_0 = 1.0$	$mb_0 = 1.2$	$mb_0 = 1.4$
0	$0.71935825 - 0.25784028\,i$	$0.80016054 - 0.21267941\,i$	$0.89645704 - 0.17253589\,i$	$1.00377455 - 0.13801622\,i$
1	$1.29062276 - 0.25811736\,i$	$1.35299556 - 0.23413835\,i$	$1.42601082 - 0.20745244\,i$	$1.50784347 - 0.17879248\,i$
2	$1.92987630 - 0.26158567\,i$	$1.97468010 - 0.25034262\,i$	$2.02826070 - 0.23728299\,i$	$2.09000500 - 0.22268827\,i$
3	$2.59924592 - 0.26030455\,i$	$2.63323242 - 0.25398401\,i$	$2.67423284 - 0.24648753\,i$	$2.72195391 - 0.23792684\,i$
5	$3.97377260 - 0.25698816\,i$	$3.99629142 - 0.25423331\,i$	$4.02365065 - 0.25091069\,i$	$4.05575648 - 0.24704466\,i$
10	$7.47160139 - 0.25296810\,i$	$7.48363819 - 0.25217484\,i$	$7.49832401 - 0.25120891\,i$	$7.51564357 - 0.25007240\,i$
15	$10.99257790 - 0.25157433\,i$	$11.00076404 - 0.25120533\,i$	$11.01076114 - 0.25075510\,i$	$11.02256429 - 0.25022409\,i$

TABLE VI. First overtone $n = 1$ QNFs ωb_0 for scalar perturbations for the Bronnikov-Ellis wormhole for several values of the angular momentum and the mass of the scalar field using the CFM.

ℓ	$mb_0 = 0$	$mb_0 = 0.2$	$mb_0 = 0.4$	$mb_0 = 0.6$
0	$0.46716556 - 2.17646191\,i$	$0.46906191 - 2.16766276\,i$	$0.47488384 - 2.14108791\,i$	$0.48505482 - 2.09619201\,i$
1	$1.25582759 - 1.70245148\,i$	$1.26145961 - 1.69485057\,i$	$1.27859466 - 1.67213708\,i$	$1.30794582 - 1.63461322\,i$
2	$2.34497715 - 1.57249831\,i$	$2.35086218 - 1.56856180\,i$	$2.36853730 - 1.55685647\,i$	$2.39805487 - 1.53769317\,i$
3	$3.39009976 - 1.53721055\,i$	$3.39499204 - 1.53499538\,i$	$3.40965523 - 1.52839415\,i$	$3.43404739 - 1.51753791\,i$
5	$5.43090081 - 1.51524731\,i$	$5.43431671 - 1.51429486\,i$	$5.44455525 - 1.51144721\,i$	$5.46158899 - 1.50673327\,i$
10	$10.46413347 - 1.50422829\,i$	$10.46600591 - 1.50395918\,i$	$10.47162139 - 1.50315267\,i$	$10.48097437 - 1.50181129\,i$
15	$15.47575755 - 1.50194589\,i$	$15.47703778 - 1.50182166\,i$	$15.48087787 - 1.50144912\,i$	$15.48727599 - 1.50082884\,i$

ℓ	$mb_0 = 0.8$	$mb_0 = 1.0$	$mb_0 = 1.2$	$mb_0 = 1.4$
0	$0.50037244 - 2.03202248\,i$	$0.52218113 - 1.94715585\,i$	$0.55270365 - 1.83962607\,i$	$0.59567461 - 1.70691857\,i$
1	$1.35067753 - 1.58289857\,i$	$1.40832928 - 1.51810061\,i$	$1.48262974 - 1.44202256\,i$	$1.57514763 - 1.35732390\,i$
2	$2.43947742 - 1.51158301\,i$	$2.49284354 - 1.47922345\,i$	$2.55812690 - 1.44147368\,i$	$2.63519525 - 1.39931666\,i$
3	$3.46809539 - 1.50263950\,i$	$3.51169079 - 1.48398519\,i$	$3.56468519 - 1.46192352\,i$	$3.62688609 - 1.43685161\,i$
5	$5.48537240 - 1.50020039\,i$	$5.51584212 - 1.49191323\,i$	$5.55291737 - 1.48195215\,i$	$5.59650057 - 1.47041133\,i$
10	$10.49405566 - 1.49993922\,i$	$10.51085246 - 1.49754225\,i$	$10.53134838 - 1.49462776\,i$	$10.55552357 - 1.49120463\,i$
15	$15.49622907 - 1.49996173\,i$	$15.50773287 - 1.49884904\,i$	$15.52178191 - 1.49749240\,i$	$15.53836956 - 1.49589379\,i$

TABLE VII. First overtone $n = 1$ QNFs ωb_0 for scalar perturbations for the wormhole spacetime described by Eq. (13) with $M/b_0 = 0.1$, for several values of the angular momentum and the mass of the scalar field using the CFM.

ℓ	$mb_0 = 0$	$mb_0 = 0.2$	$mb_0 = 0.4$	$mb_0 = 0.6$
0	$0.48215901 - 1.83934960\,i$	$0.48355134 - 1.83211141\,i$	$0.48784214 - 1.81024999\,i$	$0.49539239 - 1.77331563\,i$
1	$1.18531283 - 1.43535637\,i$	$1.18973778 - 1.42849651\,i$	$1.20321550 - 1.40798383\,i$	$1.22635308 - 1.37404779\,i$
2	$2.13978782 - 1.32436578\,i$	$2.14484682 - 1.32066795\,i$	$2.16004435 - 1.30966487\,i$	$2.18543533 - 1.29162649\,i$
3	$3.06406448 - 1.29198825\,i$	$3.06835811 - 1.28988826\,i$	$3.08122789 - 1.28362767\,i$	$3.10263958 - 1.27332322\,i$
5	$4.87885201 - 1.27072447\,i$	$4.88188492 - 1.26981683\,i$	$4.89097566 - 1.26710268\,i$	$4.90610018 - 1.26260811\,i$
10	$9.37098143 - 1.25947857\,i$	$9.37265290 - 1.25922149\,i$	$9.37766566 - 1.25845099\,i$	$9.38601480 - 1.25716938\,i$
15	$13.84985433 - 1.25707137\,i$	$13.85099838 - 1.25695263\,i$	$13.85442998 - 1.25659656\,i$	$13.86014749 - 1.25600367\,i$

ℓ	$mb_0 = 0.8$	$mb_0 = 1.0$	$mb_0 = 1.2$	$mb_0 = 1.4$
0	$0.50687537 - 1.72052831\,i$	$0.52341091 - 1.65073531\,i$	$0.54681941 - 1.56236912\,i$	$0.58009574 - 1.45346680\,i$
1	$1.26014835 - 1.32716772\,i$	$1.30593642 - 1.26821760\,i$	$1.36524947 - 1.19864836\,i$	$1.43954101 - 1.12064318\,i$
2	$2.22108946 - 1.26699755\,i$	$2.26706119 - 1.23638676\,i$	$2.32335302 - 1.20054689\,i$	$2.38987830 - 1.16034332\,i$
3	$3.13253313 - 1.25916454\,i$	$3.17081881 - 1.24140704\,i$	$3.21737287 - 1.22036208\,i$	$3.27203347 - 1.19638504\,i$
5	$4.92721862 - 1.25637588\,i$	$4.60133237 - 2.98594631\,i$	$4.62635318 - 2.96656927\,i$	$5.02590622 - 1.22790668\,i$
10	$9.39769212 - 1.25538044\,i$	$9.41268624 - 1.25308945\,i$	$9.43098258 - 1.25030310\,i$	$9.45256345 - 1.24702947\,i$
15	$13.86814819 - 1.25517478\,i$	$13.87842828 - 1.25411105\,i$	$13.89098288 - 1.25281395\,i$	$13.90580606 - 1.25128527\,i$

TABLE VIII. First overtone $n = 1$ QNFs ωb_0 for scalar perturbations for the wormhole spacetime described by Eq. (13) with $M/b_0 = 0.25$, for several values of the angular momentum and the mass of the scalar field using the CFM.

ℓ	$mb_0 = 0$	$mb_0 = 0.2$	$mb_0 = 0.4$	$mb_0 = 0.6$
0	$0.58217648 - 1.31200598\,i$	$0.58178419 - 1.30705341\,i$	$0.58074738 - 1.29211492\,i$	$0.57947867 - 1.26692340\,i$
1	$1.10576623 - 0.99897774\,i$	$1.10818210 - 0.99270181\,i$	$1.11554218 - 0.97388846\,i$	$1.12818333 - 0.94260457\,i$
2	$1.82380452 - 0.88934468\,i$	$1.82753835 - 0.88579921\,i$	$1.83876095 - 0.87522321\,i$	$1.85753019 - 0.85779732\,i$
3	$2.53427660 - 0.84472565\,i$	$2.53759327 - 0.84267946\,i$	$2.54753715 - 0.83656988\,i$	$2.56408904 - 0.82648272\,i$
5	$3.94453789 - 0.80453084\,i$	$3.94692945 - 0.80363037\,i$	$3.95409834 - 0.80093568\,i$	$3.96602715 - 0.79646673\,i$
10	$7.46522687 - 0.77201761\,i$	$7.46655166 - 0.77175658\,i$	$7.47052476 - 0.77097406\,i$	$7.47714240 - 0.76967182\,i$
15	$10.99099654 - 0.76178973\,i$	$10.99190286 - 0.76166781\,i$	$10.99462141 - 0.76130218\,i$	$10.99915090 - 0.76069321\,i$

ℓ	$mb_0 = 0.8$	$mb_0 = 1.0$	$mb_0 = 1.2$	$mb_0 = 1.4$
0	$0.57864581 - 1.23096746\,i$	$0.57916915 - 1.18343640\,i$	$0.58228934 - 1.12319399\,i$	$0.58978003 - 1.04879086\,i$
1	$1.14666028 - 0.89904448\,i$	$1.17171924 - 0.84366508\,i$	$1.20422868 - 0.77738301\,i$	$1.24504510 - 0.70180079\,i$
2	$1.88392504 - 0.83381987\,i$	$1.91802066 - 0.80370035\,i$	$1.95985689 - 0.76794601\,i$	$2.00940382 - 0.72713929\,i$
3	$2.58721432 - 0.81255726\,i$	$2.61685953 - 0.79498064\,i$	$2.65294831 - 0.77398025\,i$	$2.69537748 - 0.74981414\,i$
5	$3.98268698 - 0.79025619\,i$	$4.00403759 - 0.78234861\,i$	$4.03002761 - 0.77279927\,i$	$4.06059492 - 0.76167277\,i$
10	$7.48639830 - 0.76785275\,i$	$7.49828374 - 0.76552089\,i$	$7.51278752 - 0.76268135\,i$	$7.52989613 - 0.75934031\,i$
15	$11.00548923 - 0.75984153\,i$	$11.01363344 - 0.75874802$	$11.02357975 - 0.75741379\,i$	$11.03532354 - 0.75584020\,i$

APPENDIX B: COMPARISON OF CFM AND WKB METHODS

In Table IX we show the fundamental QNFs and the first overtone calculated using the CFM and the WKB approximation, and we see a good agreement for high ℓ. We show the relative error of the real and imaginary parts of the values obtained with the WKB method with respect to the values obtained with the CFM, which is defined by

$$\epsilon_{\mathrm{Re}(\omega)} = \frac{|\mathrm{Re}(\omega_{\mathrm{WKB}}) - \mathrm{Re}(\omega_{\mathrm{CFM}})|}{|\mathrm{Re}(\omega_{\mathrm{CFM}})|} \cdot 100\%, \quad (B1)$$

$$\epsilon_{\mathrm{Im}(\omega)} = \frac{|\mathrm{Im}(\omega_{\mathrm{WKB}}) - \mathrm{Im}(\omega_{\mathrm{CFM}})|}{|\mathrm{Im}(\omega_{\mathrm{CFM}})|} \cdot 100\%, \quad (B2)$$

where ω_{WKB} corresponds to the result obtained with the sixth order WKB method, and ω_{CFM} denotes the result with the CFM. We can observe that the error does not exceed $\approx 8.819\%$ in the imaginary part, and $\approx 2.309\%$ in the real part, for low values of ℓ. However, for high values of ℓ ($\ell = 10, 15$), the error does not exceed 0.0007% in the imaginary part, and $3.60 \times 10^{-5}\%$ in the real part. Also, as it was observed, the frequencies all have a negative imaginary part, which means that the propagation of massive scalar fields is stable in this background.

TABLE IX. QNFs ωb_0 for massive scalar field perturbations $m = 0.5$ for the wormhole spacetime described by Eq. (13) with $M/b_0 = 0.1$, $n = 0, 1$, for several values of the angular momentum ℓ of the scalar field using the CFM and the sixth order WKB approximation.

		$n = 0$		
ℓ	CFM	WKB	$\epsilon_{\mathrm{Re}(\tilde{\omega})}(\%)$	$\epsilon_{\mathrm{Im}(\tilde{\omega})}(\%)$
1	$1.48610337 - 0.42851924\,i$	$1.50406001 - 0.41070253\,i$	1.2083	4.1577
2	$2.33147670 - 0.42369524\,i$	$2.33358638 - 0.42204168\,i$	0.0905	0.3903
3	$3.20112396 - 0.42161155\,i$	$3.20146777 - 0.42132985\,i$	0.0107	0.0668
5	$4.96551051 - 0.41988141\,i$	$4.96553585 - 0.41985314\,i$	0.0005	0.0067
10	$9.41604283 - 0.41880083\,i$	$9.41604328 - 0.41879991\,i$	4.78×10^{-6}	0.0002
15	$13.88031503 - 0.41855136\,i$	$13.88031506 - 0.41855126\,i$	2.16×10^{-7}	2.39×10^{-5}

		$n = 1$		
ℓ	CFM	WKB	$\epsilon_{\mathrm{Re}(\tilde{\omega})}(\%)$	$\epsilon_{\mathrm{Im}(\tilde{\omega})}(\%)$
1	$1.21352327 - 1.39267106\,i$	$1.24154163 - 1.26985185\,i$	2.3088	8.8190
2	$2.17146134 - 1.30150131\,i$	$2.18112283 - 1.28436587\,i$	0.4449	1.3166
3	$3.09086911 - 1.27897071\,i$	$3.09292339 - 1.27587774\,i$	0.0665	0.2418
5	$4.89778582 - 1.26507565\,i$	$4.89796016 - 1.26478685\,i$	0.0036	0.0228
10	$9.38142361 - 1.25787387\,i$	$9.38142698 - 1.25786520\,i$	3.60×10^{-5}	0.0007
15	$13.85700314 - 1.25632967\,i$	$13.85700340 - 1.25632873\,i$	1.88×10^{-6}	7.48×10^{-5}

[1] L. Flamm, Beitrage zur Einsteinschen Gravitationstheorie, Phys. Z. **17**, 448 (1916).[Gen. Relativ. Gravit. **47**, 72 (2015)].

[2] A. Einstein and N. Rosen, The particle problem in the general theory of relativity, Phys. Rev. **48**, 73 (1935).

[3] C. W. Misner and J. A. Wheeler, Classical physics as geometry, Ann. Phys. (N.Y.) **2**, 525 (1957); C. W. Misner, Wormhole initial conditions, Phys. Rev. **118**, 1110 (1960).

[4] J. A. Wheeler, On the nature of quantum geometrodynamics, Ann. Phys. (N.Y.) **2**, 604 (1957); J. A. Wheeler, *Geometrodynamics* (Academic, New York, 1962).

[5] K. A. Bronnikov, Scalar-tensor theory and scalar charge, Acta Phys. Pol. B **4**, 251 (1973).

[6] H. G. Ellis, Ether flow through a drainhole—a particle model in general relativity, J. Math. Phys. (N.Y.) **14**, 104 (1973).

[7] M. S. Morris and K. S. Thorne, Wormholes in spacetime and their use for interstellar travel: A tool for teaching general relativity, Am. J. Phys. **56**, 395 (1988); M. S. Morris, K. S. Thorne, and U. Yurtsever, Wormholes, time machines, and the weak energy condition, Phys. Rev. Lett. **61**, 1446 (1988).

[8] V. Sahni and A. A. Starobinsky, The case for a positive cosmological Λ term, Int. J. Mod. Phys. D **09**, 373 (2000); S. M. Carroll, The cosmological constant, Living Rev. Relativity **4**, 1 (2001); P. J. E. Peebles and B. Ratra, The cosmological constant and dark energy, Rev. Mod. Phys. **75**, 559 (2003); P. F. Gonzales-Diaz, Stable accelerating universe with no hair, Phys. Rev. D **65**, 104035 (2002).

[9] E. Poisson and M. Visser, Thin shell wormholes: Linearization stability, Phys. Rev. D **52**, 7318 (1995).

[10] Y. Fujii and K. Maeda, *The Scalar-Tensor Theory of Gravitation* (Cambridge University Press, Cambridge, England, 2007).

[11] G. W. Horndeski, Second-order scalar-tensor field equations in a four-dimensional space, Int. J. Theor. Phys. **10**, 363 (1974).

[12] T. Kolyvaris, G. Koutsoumbas, E. Papantonopoulos, and G. Siopsis, Scalar hair from a derivative coupling of a scalar field to the Einstein tensor, Classical Quantum Gravity **29**, 205011 (2012).

[13] M. Rinaldi, Black holes with non-minimal derivative coupling, Phys. Rev. D **86**, 084048 (2012).

[14] T. Kolyvaris, G. Koutsoumbas, E. Papantonopoulos, and G. Siopsis, Phase transition to a hairy black hole in asymptotically flat spacetime, J. High Energy Phys. 11 (2013) 133.

[15] E. Babichev and C. Charmousis, Dressing a black hole with a time-dependent Galileon, J. High Energy Phys. 08 (2014) 106.

[16] C. Charmousis, T. Kolyvaris, E. Papantonopoulos, and M. Tsoukalas, Black holes in bi-scalar extensions of Horndeski theories, J. High Energy Phys. 07 (2014) 085.

[17] R. V. Korolev and S. V. Sushkov, Exact wormhole solutions with nonminimal kinetic coupling, Phys. Rev. D **90**, 124025 (2014).

[18] R. Korolev, F. S. N. Lobo, and S. V. Sushkov, General constraints on Horndeski wormhole throats, Phys. Rev. D **101**, 124057 (2020).

[19] R. Korolev, F. S. N. Lobo, and S. V. Sushkov, Kinetic gravity braiding wormhole geometries, Phys. Rev. D **102,** 104016 (2020).

[20] G. Antoniou, A. Bakopoulos, P. Kanti, B. Kleihaus, and J. Kunz, Novel Einstein–scalar-Gauss-Bonnet wormholes without exotic matter, Phys. Rev. D **101,** 024033 (2020).

[21] N. Chatzifotis, E. Papantonopoulos, and C. Vlachos, Disformal transition of a black hole to a wormhole in scalar-tensor Horndeski theory, Phys. Rev. D **105,** 064025 (2022).

[22] A. Bakopoulos, C. Charmousis, and P. Kanti, Traversable wormholes in beyond Horndeski theories, J. Cosmol. Astropart. Phys. 05 (2022) 022.

[23] A. Bakopoulos, N. Chatzifotis, C. Erices, and E. Papantonopoulos, Stealth Ellis wormholes in Horndeski theories, J. Cosmol. Astropart. Phys. 11 (2023) 055.

[24] G. Koutsoumbas, I. Mitsoulas, and E. Papantonopoulos, Quantum effects in Galileon black holes, Classical Quantum Gravity **35,** 235016 (2018).

[25] N. Chatzifotis, G. Koutsoumbas, and E. Papantonopoulos, Formation of bound states of scalar fields in AdS-asymptotic wormholes, Phys. Rev. D **104,** 024039 (2021).

[26] B. P. Abbott *et al.* (LIGO Scientific and Virgo Collaborations), Observation of gravitational waves from a binary black hole merger, Phys. Rev. Lett. **116,** 061102 (2016).

[27] B. P. Abbott *et al.* (LIGO Scientific and Virgo Collaborations), GW151226: Observation of gravitational waves from a 22-solar-mass binary black hole coalescence, Phys. Rev. Lett. **116,** 241103 (2016).

[28] B. P. Abbott *et al.* (Virgo and LIGO Scientific Collaborations), GW170104: Observation of a 50-solar-mass binary black hole coalescence at redshift 0.2, Phys. Rev. Lett. **118,** 221101 (2017).

[29] B. P. Abbott *et al.* (Virgo and LIGO Scientific Collaborations), GW170814: A three-detector observation of gravitational waves from a binary black hole coalescence, Phys. Rev. Lett. **119,** 141101 (2017).

[30] B. P. Abbott *et al.* (Virgo and LIGO Scientific Collaborations), GW170817: Observation of gravitational waves from a binary neutron star inspiral, Phys. Rev. Lett. **119,** 161101 (2017).

[31] C. V. Vishveshwara, Scattering of gravitational radiation by a Schwarzschild black-hole, Nature (London) **227,** 936 (1970).

[32] K. D. Kokkotas and B. G. Schmidt, Quasinormal modes of stars and black holes, Living Rev. Relativity **2,** 2 (1999).

[33] E. Berti, V. Cardoso, and A. O. Starinets, Quasinormal modes of black holes and black branes, Classical Quantum Gravity **26,** 163001 (2009).

[34] P. O. Mazur and E. Mottola, Gravitational condensate stars: An alternative to black holes, Universe **9,** 88 (2023).

[35] M. S. Morris, K. S. Thorne, and U. Yurtsever, Wormholes, time machines, and the weak energy condition, Phys. Rev. Lett. **61,** 1446 (1988).

[36] T. Damour and S. N. Solodukhin, Wormholes as black hole foils, Phys. Rev. D **76,** 024016 (2007).

[37] R. A. Konoplya and A. Zhidenko, Quasinormal modes of black holes: From astrophysics to string theory, Rev. Mod. Phys. **83,** 793 (2011).

[38] V. Cardoso, E. Franzin, and P. Pani, Is the gravitational-wave ringdown a probe of the event horizon?, Phys. Rev. Lett. **116,** 171101 (2016).

[39] B. Holdom and J. Ren, Not quite a black hole, Phys. Rev. D **95,** 084034 (2017).

[40] R. A. Konoplya and A. V. Zhidenko, Decay of massive scalar field in a Schwarzschild background, Phys. Lett. B **609,** 377 (2005).

[41] R. A. Konoplya and A. Zhidenko, Stability and quasinormal modes of the massive scalar field around Kerr black holes, Phys. Rev. D **73,** 124040 (2006).

[42] S. R. Dolan, Instability of the massive Klein-Gordon field on the Kerr spacetime, Phys. Rev. D **76,** 084001 (2007).

[43] O. J. Tattersall and P. G. Ferreira, Quasinormal modes of black holes in Horndeski gravity, Phys. Rev. D **97,** 104047 (2018).

[44] A. Aragón, P. A. González, E. Papantonopoulos, and Y. Vásquez, Anomalous decay rate of quasinormal modes in Schwarzschild-dS and Schwarzschild-AdS black holes, J. High Energy Phys. 08 (2020) 120.

[45] R. D. B. Fontana, P. A. González, E. Papantonopoulos, and Y. Vásquez, Anomalous decay rate of quasinormal modes in Reissner-Nordström black holes, Phys. Rev. D **103,** 064005 (2021).

[46] P. A. González, E. Papantonopoulos, J. Saavedra, and Y. Vásquez, Quasinormal modes for massive charged scalar fields in Reissner-Nordström dS black holes: Anomalous decay rate, J. High Energy Phys. 06 (2022) 150.

[47] A. Aragón, R. Bécar, P. A. González, and Y. Vásquez, Massive Dirac quasinormal modes in Schwarzschild–de Sitter black holes: Anomalous decay rate and fine structure, Phys. Rev. D **103,** 064006 (2021).

[48] K. Destounis, R. D. B. Fontana, and F. C. Mena, Accelerating black holes: Quasinormal modes and late-time tails, Phys. Rev. D **102,** 044005 (2020).

[49] A. Aragón, P. A. González, E. Papantonopoulos, and Y. Vásquez, Quasinormal modes and their anomalous behavior for black holes in $f(R)$ gravity, Eur. Phys. J. C **81,** 407 (2021).

[50] A. Aragón, P. A. González, J. Saavedra, and Y. Vásquez, Scalar quasinormal modes for $2 + 1$-dimensional Coulomb-like AdS black holes from nonlinear electrodynamics, Gen. Relativ. Gravit. **53,** 91 (2021).

[51] R. Bécar, P. A. González, F. Moncada, and Y. Vásquez, Massive scalar field perturbations in Weyl black holes, Eur. Phys. J. C **83,** 942 (2023).

[52] R. Bécar, P. A. González, E. Papantonopoulos, and Y. Vásquez, Massive scalar field perturbations of black holes surrounded by dark matter, Eur. Phys. J. C **84,** 329 (2024).

[53] R. A. Konoplya and C. Molina, The ringing wormholes, Phys. Rev. D **71,** 124009 (2005).

[54] R. A. Konoplya and A. Zhidenko, Wormholes versus black holes: Quasinormal ringing at early and late times, J. Cosmol. Astropart. Phys. 12 (2016) 043.

[55] M. S. Churilova, R. A. Konoplya, and A. Zhidenko, Arbitrarily long-lived quasinormal modes in a wormhole background, Phys. Lett. B **802,** 135207 (2020).

[56] R. A. Konoplya, How to tell the shape of a wormhole by its quasinormal modes, Phys. Lett. B **784,** 43 (2018).

[57] J. L. Blázquez-Salcedo, X. Y. Chew, and J. Kunz, Scalar and axial quasinormal modes of massive static phantom wormholes, Phys. Rev. D **98,** 044035 (2018).

[58] P. A. González, E. Papantonopoulos, Á. Rincón, and Y. Vásquez, Quasinormal modes of massive scalar fields in four-dimensional wormholes: Anomalous decay rate, Phys. Rev. D **106,** 024050 (2022).

[59] B. Azad, J. L. Blázquez-Salcedo, X. Y. Chew, J. Kunz, and D. h. Yeom, Polar modes and isospectrality of Ellis-Bronnikov wormholes, Phys. Rev. D **107,** 084024 (2023).

[60] F. S. Khoo, B. Azad, J. L. Blázquez-Salcedo, L. M. González-Romero, B. Kleihaus, J. Kunz, and F. Navarro-Lérida, Quasinormal modes of rapidly rotating Ellis-Bronnikov wormholes, Phys. Rev. D **109,** 084013 (2024).

[61] T. Karakasis, E. Papantonopoulos, Z. Y. Tang, and B. Wang, Black holes of $(2 + 1)$-dimensional $f(R)$ gravity coupled to a scalar field, Phys. Rev. D **103,** 064063 (2021).

[62] T. Karakasis, E. Papantonopoulos, Z. Y. Tang, and B. Wang, Exact black hole solutions with a conformally coupled scalar field and dynamic Ricci curvature in f(R) gravity theories, Eur. Phys. J. C **81,** 897 (2021).

[63] Z. Y. Tang, B. Wang, and E. Papantonopoulos, Exact charged black hole solutions in D-dimensions in $f(R)$ gravity, Eur. Phys. J. C **81,** 346 (2021).

[64] V. De Falco, E. Battista, S. Capozziello, and M. De Laurentis, Reconstructing wormhole solutions in curvature based extended theories of gravity, Eur. Phys. J. C **81,** 157 (2021).

[65] T. Karakasis, E. Papantonopoulos, and C. Vlachos, f(R) gravity wormholes sourced by a phantom scalar field, Phys. Rev. D **105,** 024006 (2022).

[66] K. A. Bronnikov, Scalar fields as sources for wormholes and regular black holes, Particles **1,** 56 (2018).

[67] G. C. Samanta and N. Godani, Validation of energy conditions in wormhole geometry within viable $f(R)$ gravity, Eur. Phys. J. C **79,** 623 (2019).

[68] C. Muller, in *Lecture Notes in Mathematics: Spherical Harmonics* (Springer-Verlag, Berlin-Heidelberg, 1966).

[69] E. W. Leaver, An analytic representation for the quasi normal modes of Kerr black holes, Proc. R. Soc. A **402,** 285 (1985).

[70] E. W. Leaver, Quasinormal modes of Reissner-Nordstrom black holes, Phys. Rev. D **41,** 2986 (1990).

[71] H. P. Nollert, Quasinormal modes of Schwarzschild black holes: The determination of quasinormal frequencies with very large imaginary parts, Phys. Rev. D **47,** 5253 (1993).

[72] V. Cardoso, J. P. S. Lemos, and S. Yoshida, Scalar gravitational perturbations and quasinormal modes in the five-dimensional Schwarzschild black hole, J. High Energy Phys. 12 (2003) 041.

[73] R. A. Konoplya and A. Zhidenko, Massive charged scalar field in the Kerr-Newman background I: Quasinormal modes, late-time tails and stability, Phys. Rev. D **88,** 024054 (2013).

[74] M. Richartz and D. Giugno, Quasinormal modes of charged fields around a Reissner-Nordström black hole, Phys. Rev. D **90,** 124011 (2014).

[75] A. Chowdhury and N. Banerjee, Quasinormal modes of a charged spherical black hole with scalar hair for scalar and Dirac perturbations, Eur. Phys. J. C **78,** 594 (2018).

[76] R. Bécar, P. A. González, and Y. Vásquez, Quasinormal modes of a charged scalar field in Ernst black holes, Eur. Phys. J. C **83,** 75 (2023).

[77] K. A. Bronnikov, R. A. Konoplya, and T. D. Pappas, General parametrization of wormhole spacetimes and its application to shadows and quasinormal modes, Phys. Rev. D **103,** 124062 (2021).

[78] S. Aneesh, S. Bose, and S. Kar, Gravitational waves from quasinormal modes of a class of Lorentzian wormholes, Phys. Rev. D **97,** 124004 (2018).

[79] P. Dutta Roy, S. Aneesh, and S. Kar, Revisiting a family of wormholes: Geometry, matter, scalar quasinormal modes and echoes, Eur. Phys. J. C **80,** 850 (2020).

[80] B. Mashhoon, Quasinormal modes of black holes. The improved semianalytic approach, Phys. Rev. D **96,** 024011 (2017).

[81] B. F. Schutz and C. M. Will, Black hole normal modes: A semianalytic approach, Astrophys. J. Lett. **291,** L33 (1985).

[82] S. Iyer and C. M. Will, Black hole normal modes: A WKB Approach. 1. Foundations and application of a higher order WKB analysis of potential barrier scattering, Phys. Rev. D **35,** 3621 (1987).

[83] R. A. Konoplya, Quasinormal behavior of the d-dimensional Schwarzschild black hole, and higher order WKB approach, Phys. Rev. D **68,** 024018 (2003).

[84] J. Matyjasek and M. Opala, Quasinormal modes of black holes. The improved semianalytic approach, Phys. Rev. D **96,** 024011 (2017).

[85] R. A. Konoplya, A. Zhidenko, and A. F. Zinhailo, Higher order WKB formula for quasinormal modes and grey-body factors: Recipes for quick and accurate calculations, Classical Quantum Gravity **36,** 155002 (2019).

[86] Y. Hatsuda, Quasinormal modes of black holes, and Borel summation, Phys. Rev. D **101,** 024008 (2020).